See folder for MEMO to Browning fm. Verma 10-26-84

Theoretical Modeling of Hole-to-Surface Resistivity Measurements For Hazardous Waste Analysis

by

Jeffrey J. Daniels
U.S. Geological Survey
Denver, Colorado

and

H. Truman Holcombe*
Geotechnical Exploration Inc.
San Diego, California

U.S. Geological Survey Open File Report

* presently with SOHIO Petroleum, Dallas, Texas

8412040195 841026
PDR WASTE
WM-16 PDR

Abstract

A computer modeling technique for buried electrode resistivity surveys is presented. The technique uses finite elements, which allows modeling of virtually any geometric distribution of rock resistivities that could be present in toxic waste, or nuclear waste field sites.

Computer models for shallow resistive and conductive bodies illustrate the effectiveness of computer modeling for determining the anomaly size and shape that can be expected from hole-to-surface resistivity measurements for various resistivity contrasts related to toxic waste anomalies. Similar examples for deeply buried bodies show the effectiveness of the models for analyzing anticipated targets in nuclear waste site appraisal. Results of these tests also show that in general, the optimum position of the electrical source is below the target body. Models of a deeply buried fracture zone (low resistivity) contained in a resistive layer (eg. salt) yields a large anomaly that could be easily detected with hole-to-surface resistivity measurements.

Introduction

The detection of geologic inhomogenities near a hazardous waste storage area will require the use of techniques that do not jeopardize the structural integrity of the rock formation with concentrated drilling. Although surface geophysical techniques can be used to detect near-surface rock properties, hole-to-surface resistivity measurements improve the depth penetration and resolution of resistivity, while minimizing the number of drill holes needed to evaulate a potential waste repository site. Hole-to-surface resistivity measurements have been successfully tested in shallow volcanic rocks (Daniels, 1978), and metamorphic rocks (Daniels, 1984)) and in a deeply buried evaporite sequence (Daniels, 1982).

The hole-to-surface resistivity array is illustrated in Figure 1. Hole-to-surface measurements are made by placing a pole, or bipole, source down a borehole and measuring the resulting distribution of the electric potential on the surface. Previous field studies have shown that the optimum source-receiver configuration for many applications consists of a pole source in the borehole, and orthogonal potential dipole measurements on the surface. A dipole potential receiver, consisting of closely spaced poles, enables the interpreter to calculate the approximate total electric field. Non-radial components of the electric field are zero in a homogenous or laterally isotropic earth. If lateral inhomogeneities are present in the geoelectric section, then the direction of the electric current emanating from a buried current source is not

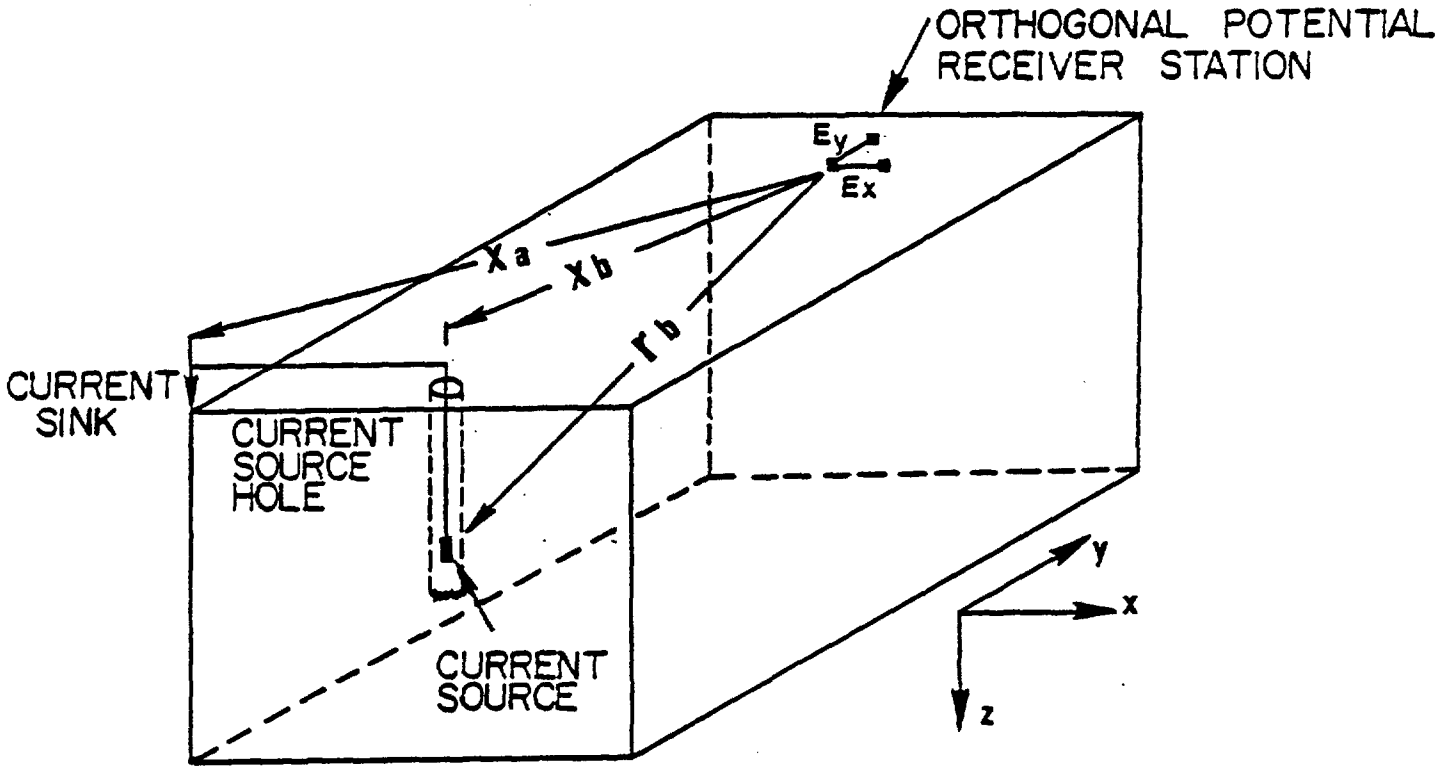

Figure 1. The hole-to-surface resistivity array for a pole source and orthogonal potential dipole array.

radial, and it is necessary to measure two orthogonal components of the potential in order to measure the total electric field. Theoretical studies of surface potentials due to in-hole current sources have been described by Alfano (1962), Merkel (1971), Merkel and Alexander (1971), Snyder and Merkel (1973), and Daniels (1977, 1978).

Theoretical solutions for buried electrodes in a one- or two-layered medium have been given by Daknov (1959), and Van Norstrand and Cook (1966). Daknov (1959) has shown example curves for the normal and lateral well logging arrays in the presence of a resistive layer. Schlumberger departure curves (1972) also use models of three-layer cases for various well logging arrays.

A theoretical solution to the problem of a buried current electrode in a three-layered earth with a surface receiver bipole was first presented by Alfano (1962). Analytic models for a buried source and surface receiver for a sphere and three-layered earth models were given by Snyder and Merkel (1973) and Merkel and Alexander (1971). Daniels (1977, 1978) has presented the solutions for buried electrodes in an n-layered earth, and for an arbitrarily shaped three dimensional body in a homogenous halfspace.

All of the models mentioned above are limited in the complexities that can be included in the models. The model used in the study presented in this paper (developed by Holcombe (1983) under contract to the U.S. Geological Survey)incorporates several basic model elements (topography, layered earth, multiple three dimensional bodies) into a single model that can be used to simulate complex geologic conditions. In addition, the model can

be used to simulate any electrode configuration (eg. hole-to-hole, hole-to-surface, etc.). However, the model results presented in this paper are restricted to the hole-to-surface array using a buried pole source, and total field surface receiver. The models were chosen to illustrate the hole-to-surface resistivity response for various depths and positions of the body representing the resistivity contrast with respect to the current source.

General Description of the Model

The purpose of this algorithm is to provide a capability to calculate direct current resistivity responses for realistically complex three-dimensional earth models, that may include arbitrary topography at the earth-air interface. The algorithm can be set up to simulate virtually any surface or subsurface configuration of current and potential electrodes. The algorithm is currently configured to calculate responses for (1) the Schlumberger, (2) the dipole-dipole, (3) the hole-to-hole, and (4) the hole-to-surface electrode configurations.

The computer algorithm makes use of the finite element method to calculate the electric potential distribution in the earth about an array of point current sources. The elements have a convenient hexahedral (rectangular prism) shape to facilitate the construction of a complex, discrete earth model. The near-surface layers of elements can be distorted, using an isoparametric coordinate transformation, to accomodate topography in the model. This is illustrated in Figure 2, where the dashed

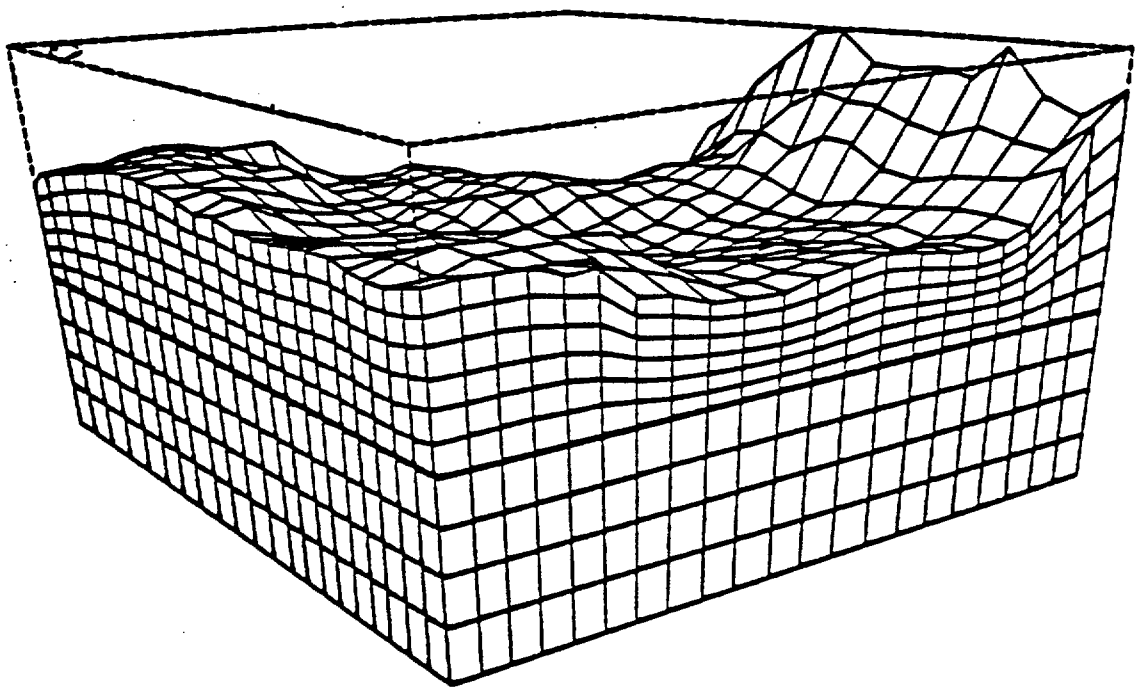

Figure 2. Basic model configuration. The dashed box is the boundary of the original undistorted geometry. The solid-line grid represents the distorted isoparmaetric element geometry. The heavy solid line is the horizon separating the distorted elements above from the undistorted ones below.

box represents the original undistorted geometry and the solid line grid is the distorted isoparametric element geometry. The geometric change is accomplished by using a coordinate transformation which translates the coordinates of the corners of the elements (which are the locations of the finite element nodes) vertically downward an appropriate distance. The heavy solid line is an arbitrarily determined horizon which separates the distorted elements from the undistorted ones.

The term "isoparametic" refers to the order of the polynomial form (ie., linear, quadratic, etc.) used to relate the transformed to the untransformed coordinates. If it is the same order as the polynomial used to approximate the variation of the parameter of interest within a finite element, then the distorted element is called "isoparametric". The terms "subparametric" and "superparametric" are used for transformations of lower or higher order, respectively.

Theoretical Development

The theoretical resistivity development follows that of Pridmore and others (1981), with the addition of isoparametric finite elements near the surface of the earth model to simulate topography. Isoparametric elements can be distorted to incorporate an irregular surface without loss of generality.

The domain equation is the steady-state equation of continuity of current density:

$$\vec{\nabla} \cdot \vec{J}_c = 0 \qquad (1)$$

where $\vec{J}_c$ is the conduction current density within an arbitrary volume of the earth when current sources are absent. It is assumed that the conductivity of the earth is isotropic and a function of position only. Therefore, Ohm's Law ($\vec{J}_c = \vec{E}$) can be substituted into equation (1), and since $\vec{E} = -\vec{\nabla}\phi$, then:

$$-\vec{\nabla}\cdot\sigma\vec{\nabla}\phi = 0 \qquad (2)$$

where ϕ is the scalar electric potential. When the volume of earth under investigation contains sources of diverging current, then

$$-\vec{\nabla}\cdot\sigma\vec{\nabla}\phi = \vec{\nabla}\cdot\vec{J}_s \qquad (3)$$

where $\vec{J}_s$ is the current density due to the sources.

The finite element method has a long history of success in a wide variety of applications (Huebner, 1975, p.13-14) and its validity for the classic Poisson problem defined by equation (3) is well established. The domain for the finite element numerical solution is a model where topography is superimposed upon an otherwise rectangular prism shaped volume of earth. This model is divided into hexahedral or distorted hexahedral elements as shown in Figure 2. The distorted elements are mapped onto a regular hexahedral array by a vertical coordinate transformation.

The true solution within each hexahedral finite element (see Figure 3) is approximated by a trial function of the form:

$$\phi_e(u,v,w) = \sum_{i=1}^{8} N_i(u,v,w)\,\phi_i \qquad (4)$$

where the ϕ_i's are the nodal values of the electric potential and the N_i's are the shape functions defined as

$$N_i(u,v,w) = \frac{1}{8a^2b^2c^2}(a^2+uu_i)(b^2+vv_i)(c^2+ww_i) \qquad (5)$$

where u,v, and w are Cartesian coordinates in the transformed,

undistorted finite element space, u_i, v_i, and w_i are the nodal values and 2a, 2b, and 2c are the u, v, and w dimensions of the element. This type of element is an isoparametric tri-linear element of the serendipity class (Huebner, 1975, p. 179-191). The variational method is chosen for the derivation of the finite element matrix, although other finite element methods will result in an identical formulation.

If the equation that the true solution satisfies is known, then the trial solution given in equation(4) may be forced to satisfy it. In this case, equation (3) may be written for the nth finite element in the following operator form:

$$L\phi = f \qquad (6)$$

where L is the Laplacian operator $[\vec{\nabla}\cdot\sigma\vec{\nabla}]$ and f=0, or $f=\vec{\nabla}\cdot\vec{J}_s$, depending on whether or not the nth element contains a source. The minimum theorem (see Mikhlin and Smolitskiy, 1967, p. 147-155) states that the solution of (6) minimizes the functional, expressed in inner product form,

$$F_n(\phi) = \langle L\phi, \phi\rangle - 2\langle \phi, f\rangle \qquad (7)$$

provided that the following conditions are met:

1. The operator L is self-adjoint and positive definite. This has been proven by Pridmore and others (1978).

2. ϕ and f are elements of the same Hilbert space. They must be members of the subspace of all functions which have continuous first derivatives within the nth element.

The inner product notation in equation (7) is defined by

$$\langle a,b\rangle = \int_{V_n} (a\cdot b)\, dV_n$$

which is the volume integral over the nth element of the dot product of functions a, and b. Therefore, for the nth element

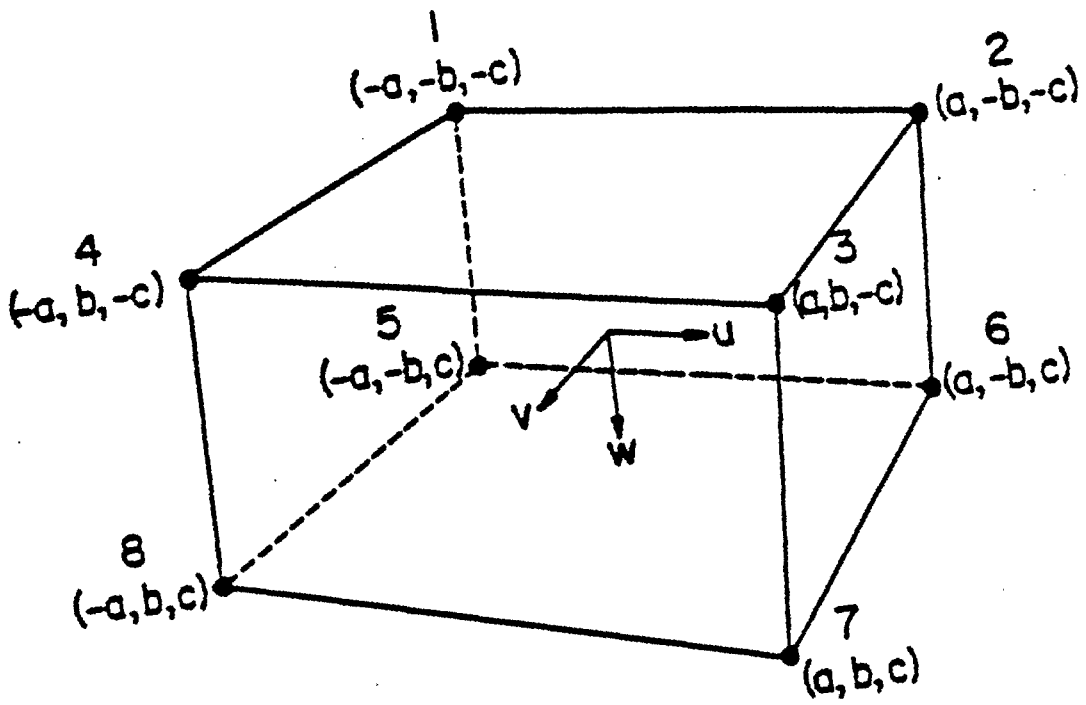

Figure 3. Coordinate configuration and node numbering scheme for hexahedral finite element.

$F_n(\phi)$ is minimum if the first variation is zero, that is

$$\left.\frac{\partial F_n(\phi)}{\partial \phi}\right|_{\phi_1} = \left.\frac{\partial F_n(\phi)}{\partial \phi}\right|_{\phi_2} = \cdots = \left.\frac{\partial F_n(\phi)}{\partial \phi}\right|_{\phi_8} = 0 \qquad (8)$$

where $\phi_1 \ldots \phi_8$ are the nodal values of the potential in the nth element. Equation (8) may be evaluated as follows. Integrating the first term in equation (7) by parts yield:

$$\langle -\vec{\nabla}\cdot\sigma_n\vec{\nabla}\phi, \phi\rangle = \langle \sigma_n\vec{\nabla}\phi, \vec{\nabla}\phi\rangle - \int_{S_n}\sigma_n\phi\frac{\partial\phi}{\partial\eta}\,ds \qquad (9)$$

where the surface integral is computed over a closed volume containing the domain which we define to be the nth finite element. $\frac{\partial\phi}{\partial\eta}$ is the spatial derivative of ϕ normal to the bounding plane. Therefore,

$$\langle -\vec{\nabla}\cdot\sigma\vec{\nabla}\phi, \phi\rangle = \sum_n\int_{V_n}\sigma_n(\vec{\nabla}\phi)^2\,dV_n - \sum_n\int_{S_n}\sigma_n\phi\frac{\partial\phi}{\partial\eta}\,dS_n \qquad (10)$$

Continuity of current within the conducting model requires that the internal surface integral components of adjoining elements cancel one another. At the external surface where the homogenous Nuemann boundry condition applies, the component of the surface integral is zero by definition. The surface integral at the boundries where the known inhomogenous Dirchlet condition applies is, by definition, constant and has no part in determining the miniumum of the functional. Therefore, the surface integral terms neeed not be considered, and

$$F_n(\phi) = \int_{V_n}[\sigma_n(\vec{\nabla}\phi)^2 - 2\phi\vec{\nabla}\cdot\vec{J}_s(u,v,w)]\,dV_n \qquad (11)$$

Therefore, the first variation of the functional at node 1 becomes:

$$\left.\frac{\partial F_n(\phi)}{\partial \phi}\right|_{\phi_1} = -2\int_{V_n} N_1 \vec{\nabla}\cdot\vec{J}_s(u,v,w)\,dV_n$$
$$+2\sigma_n\int_{V_n}\left[\frac{\partial N_1}{\partial u}\left(\frac{\partial N_1}{\partial u}+\ldots+\frac{\partial N_8}{\partial u}\right)+\frac{\partial N_1}{\partial v}\left(\frac{\partial N_1}{\partial v}+\ldots+\frac{\partial N_8}{\partial v}\right)\right.$$
$$\left.+\frac{\partial N_1}{\partial w}\left(\frac{\partial N_1}{\partial w}+\ldots+\frac{\partial N_8}{\partial w}\right)\right](\phi_1+\ldots+\phi_8)\,dV_n \qquad (12)$$

where σ_n is the isotropic conductivity within the homogenous nth element, V_n is the volume of the element, and $\vec{J}_s$ (u, v, w) is the current density within the undistorted element.

Topography is incorporated into the earth model by mapping the regular hexahedral elements onto a contiguous array of irregularly shaped elements as shown in Figure 2. This is done in the usual fashion, so that equation (12) becomes:

$$\left.\frac{\partial F_n(\phi)}{\partial \phi}\right|_{\phi_1} = -2\int_{V_n} N_1 \vec{\nabla}\cdot\vec{J}_s(u,v,w)(\det J_{uvw})\,dV_n$$
$$+2\sigma_n\int_{V_n}\left[\frac{\partial N_1}{\partial u}\left(\frac{\partial N_1}{\partial u}+\ldots+\frac{\partial N_8}{\partial u}\right)+\frac{\partial N_1}{\partial v}\left(\frac{\partial N_1}{\partial v}+\ldots+\frac{\partial N_8}{\partial v}\right)\right. \qquad (13)$$
$$\left.+\frac{\partial N_1}{\partial w}\left(\frac{\partial N_1}{\partial w}+\ldots+\frac{\partial N_8}{\partial w}\right)\right](\phi_1+\ldots+\phi_8)(\det J_{uvw})\,dV_n$$

where

$$\det J_{uvw} = \begin{vmatrix} \frac{\partial x}{\partial u} & \frac{\partial x}{\partial v} & \frac{\partial x}{\partial w} \\ \frac{\partial y}{\partial u} & \frac{\partial y}{\partial v} & \frac{\partial y}{\partial w} \\ \frac{\partial z}{\partial u} & \frac{\partial z}{\partial v} & \frac{\partial z}{\partial w} \end{vmatrix} \qquad (14)$$

In this case, we use a linear transformation in the vertical direction, with the node locations in the hexahedral elements

translated vertically. Therefore,

$$\det J_{uvw} = \begin{vmatrix} 1 & 0 & 0 \\ 0 & 1 & 0 \\ 0 & 0 & \frac{\partial z}{\partial w} \end{vmatrix} \qquad (15)$$

In order to facilitate integration, the shape function defined for the trial solution is also used for making the transformation, and

$$Z = \sum_{i=1}^{8} N_i(u,v,w) Z_i \qquad (16)$$

where the z_i's are the vertical coordinates of the models in the distorted element.

The boundry conditions imposed on the finite element model developed for this study are the homogenous Neumann condition at the earth-air interface, and an inhomogenous Dirchlet condition at the subsurface external model boundaries (Pridmore and others, 1981). Pridmore and others (1981) simply applied the potentials calculated for an appropriate homogenous half-space. The model algorithm described in this paper utilizes an image method solution to calculate the potential distribution about an array of point current sources in a layered earth. The sources can be at the surface or buried in one of the layers. This calculation, along with a topographic adjustment factor (V_t), based on the empirical behavior of the electric potential near a simple topographic feature, is used as both a starting point for the iterative matrix solution described below and the fixed model boundary condition described previously.

Inhomogenous Dirchlet boundaries are incorrect from a theoretical point of view, since an assumed value of the electric

potential is assumed at some fixed, pre-determined distance form the sources. Probably the best boundary condition for models of finite dimension is the following asymptotic condition used by Dey and Morrison (1979):

$$\frac{\partial \phi}{\partial \eta} + \frac{\phi \cos\theta}{r_s} = 0 \qquad (17)$$

where θ is the angle between the radial vector from the source, r_s, and the outward normal spatial coordinate, η. This condition imposes the asymptotic 1/r behavior of the potential at large distances from the source on the bounding planes of the earth model. Implementing this condition requires either (1) using a different finite element formulation at the boundaries which explicitly includes equation (17) (see Pridmore, 1978), or (2) appropriately adjusting the potential at the bounding nodes during iterative solution process to be described later (see Norrie and de Vries, 1978, p.213). Unfortunately, procedure (1) requires a considerable programming effort, which has not been attempted, and procedure (2) results in a significant increase in the number of iterations, and the computer time required to arrive at a good solution.

The method of calculating the initial potential distribution is described in detail by Daniels, 1978. However, the essential elements of the development are reproduced here for continuity and completeness. The general expression for the potential ϕ_m at point m, contained in layer i, due to a current source at A, contained in layer j, is

$$\phi_m = \frac{I\rho_j V_t}{4\pi}\left\{\frac{1}{AM} + \int_0^\infty (\alpha_i e^{\lambda z(AM)} + \beta_i e^{-\lambda z(AM)}) J_0(\lambda r_{am}) d\lambda \quad (18)\right.$$

where α_i and β_i are the coefficients for the disturbing potential due to the layering, z(AM) is the vertical distance between the current source and potential receiver, AM is the distance between electrodes A and M, AM is the radial distance from A to M, ρ_j is the resistivity of layer j, λ is the dummy variable of integration, and J_0 is the zeroth order Bessel function of the first kind. The positions of the source and receiver with respect to the layers are shown in Figure 4. The derivation of α_i and β_i from layer interface boundary conditions is given by Daniels(1978).

The potential distribution for a source position at the surface cna be calculated from expression identical to equation (18) except that the 4π in the right-hand side of the denominator becomes 2π. This is because the solid angle subtending the source is only 2π steradians when it is at the surface. A digital filter technique, described by Anderson (1975), is used to perform the numerical integration in equation (18). The term V_t in equation (18) is given by

$$V_t = 1 + \frac{e_s - e}{r_s} \quad (19)$$

where e_s is the surface elevation of the source point, e is the surface elevation at the point where the potential is calculated, and r_s is the straight line separation distance between the source and the point where the potential is calculated. It is based on the asymptotic behavior of the electric potential far removed from a source near a ramp slope, shown in the lower part

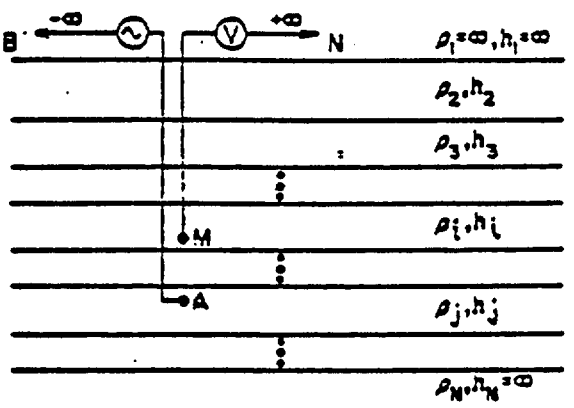

Figure 4. Electrode array for buried source potential distribution calculation. Resistivities and layer thicknesses are indicated by and h, respectively. "A" is the current electrode and M is the potential electrode. (Daniels, 1978)

of Figure 5. This behavior was determined from a number of calcualted responses for models containing ramp slope features like that shown in Figure 5. Incorporating the analytic multiplier V_t in the original calcualtion of the potential array, equation (18) gave a reasonable approximation of the behavior calculated in the test models at grid locations relatively far removed from the ramp slope, but should be viewed as a first order correction. Equation (19) describes the empirical relationship between the potentials calculated for the ramp slope (solid line) and a flat surface (dotted line) at distances far removed for the slope (see Figure 5). This relationship holds (for relatively small elevation changes) whether or not the slope is up or down with respect to the source.

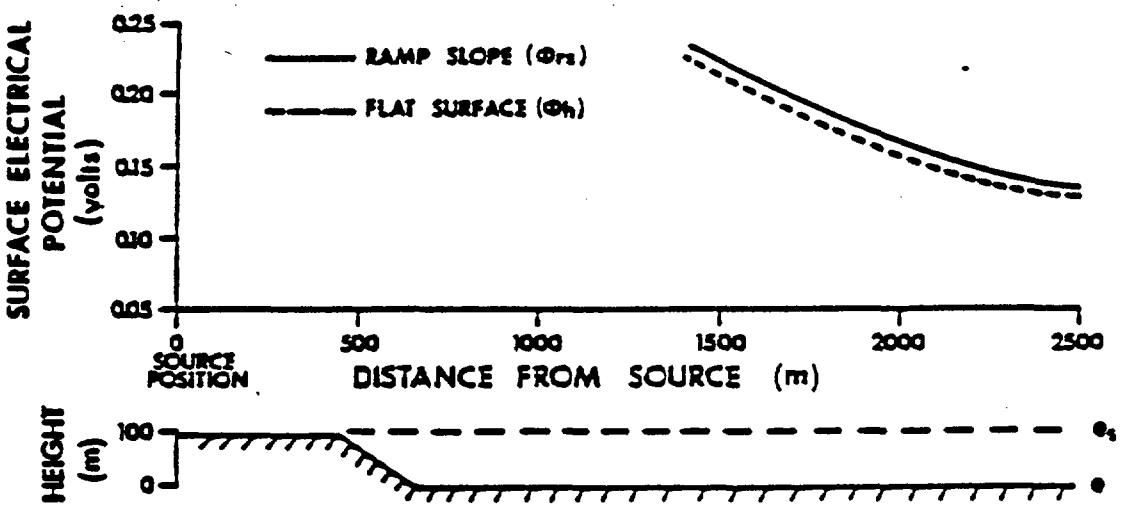

Figure 5. Illustration of asymptotic behavior of electric potential far remeoved from a unit point source near a ramp slope. The empirically determined relationship is given by $\emptyset_{rs}=\emptyset_h(1+(e_s - e)/r_s)$.

Numerical Solution

The evaluation of the integrals in the functional (equation 2) are analytic because of the choice of linear functions for both the trial solution and the coordinate transformation. Minimization of the functional (requiring the first variation to be zero) results in an 8 x 8 matrix equaiton of the form:

$$\begin{bmatrix} a_{11} & a_{12} & \cdots & a_{18} \\ a_{21} & a_{22} & & \vdots \\ \vdots & & \ddots & \vdots \\ a_{81} & \cdots & & a_{88} \end{bmatrix} \cdot \begin{bmatrix} \phi_1 \\ \phi_2 \\ \\ \phi_8 \end{bmatrix} = \begin{bmatrix} s_1 \\ s_2 \\ \\ s_8 \end{bmatrix} \qquad (20)$$

where the coefficient matrix $[a_{ij}]$ is symmetric and is usually referred to as the element matrix. For the simple hexahedral element (equation 1), there are eight independent coefficients. In the distorted element (equation),there are 18 independent coefficients. Normally, the finite element matrix equations are assembled into a global matrix and then solved by one of the matrix inversion techniques commonly used. However, because of the very large number of elements (sometimes 50,000 or more are required) the memory requirement for such an inversion far exceeds the core memory available on even the largest computer. Therefore, a successive node iterative solution technique was used, whcih solves only the matrix equations for elements adjacent to a given node at any particular time. This allows a reduction in the memory required, but greatly increases the running time. The solution method chosen is usually called the successive point over-relaxation (SPOR) method. It is described in detail in many texts (eg. Ames, 1977, p.119-125). A brief

description of the method follows.

An initial guess at the solution vector is substituted into an m x m system of equations

$$\begin{bmatrix} a_{11} & a_{12} & \cdots & a_{1m} \\ a_{21} & a_{22} & & \vdots \\ \vdots & & \ddots & \vdots \\ a_{m1} & \cdots & & a_{mm} \end{bmatrix} \quad \begin{bmatrix} \phi_1 \\ \phi_2 \\ \\ \phi_m \end{bmatrix} \quad \begin{bmatrix} S_1 \\ S_2 \\ \\ S_m \end{bmatrix} \qquad (21)$$

and successive iterations proceed in the following manner. At iteration n, the i-th row

$$\sum_{j=1}^{m} a_{ij}\phi_j = \sum_{j=1}^{m} S_j \qquad (22)$$

is solved for the n+1 value of ϕ_k for $1 \leq k \leq m$, yielding

$$\phi_k^{n+1} = \left\{ \left[\frac{\sum_{j=1}^{m} S_j - \sum_{j=1}^{k-1} a_{ij}\phi_j^n - \sum_{j=k+1}^{m} a_{ij}\phi_j^n}{a_{ik}} \right] - \phi_k^n \right\} W_n + \phi_k^n \qquad (23)$$

where the ϕ_j^n are the values of ϕ_j calculated in iteration n and W_n is a factor called the acceleration parameter. If $1<W_n<2$, this process is called over relaxation, and the rate of convergence is dependent on what values of W_n is selected. The term inside the large brackets, $\{\ \}$, is called the residual. Its behavior in successive iterations determines whether or not the process is converging to a solution, but not necessarily the rate of convergence. For very large systems of equations the process uses excessive computer time, so it is important to determine an optimum value for W_n which gives a maximum rate of convergence.

When the matrix has consistent ordering (property "A" in Ames, 1977, p.120), then an optimum values of W_n may be determined theoretically. Unfortunately, the finite element

formulation used here does not have this property. However, Carre (1961) and Pridmore (1978) have suggested that W_n should be the maximum value for which the successive residuals calculated do not exhibit an oscillatory behavior.

The following technique has been used in this application: (1)An initial value is chosen which has experimentally been determined to be less than but close to the optimum. (2)The maximum residual is tested after each iteration, and if it is less than that of the previous iteration, then W_n is incremented upward by a predetermined amount. If the maximum residual is greater, then W_n is incremented downward. The initial value is typically about 1.5, the upward increment is 0.005, and the downward increment is 0.05.

Another important consideration is the choice of an optimum method of assembly of a local matrix equaiton from the appropriate element matrices of the SPOR process. Desai and Abel (1971) and others state that empirical evidence suggests that a nodal assemblage is best when using an iterative scheme for the solution. The nodal assembly process is discussed in numerous texts (eg. Norrie and de Vries, 1978) but a brief description of what has been implemented in this application is included here for continuity.

Each node in the finite element array is included in eight adjacent elements if it is an interior node, and four adjacent elements if it is an exterior node. A nodal assemblage is accomplished by grouping into a single row of the nodal matrix the eight (or four) rows in the respective adjacent element

matrices in which the coefficient for the node is contained in the diagonal position. In the final analysis, each row of the nodal matrix yields an interpolation of the nodal potential from each of the surrounding 26 nodal values during each iteration, which is equivalent to a 27 point finite difference approximation.

In many approximate solution techniques, such as the finite difference approach of Dey and Morrison (1976), one can use a point current source in the formulation, where the divergence of the current density in equations (12) and (13) can be replaced with

$$\vec{\nabla}\cdot\vec{J}_s = I\,\delta(\vec{r}-\vec{r}_o) \qquad (24)$$

where $\delta(r-r_o)$ is the three dimensional Diric delta function, and I is the magnitude of a point current source at position r_o. However, the variational method used to derive the finite element matrix equations does not allow this form, since the Dirac delta function does not have a continuous first derivative, which is required by the minimum theorem (see Mikhlin and Smolitskiy, 1967, p. 147-155). In general, one needs a functional form for $\vec{\nabla}\cdot\vec{J}_s$ that meets the criteria for the minimum theorem and approximates as closely as possible the current flow from a point source. However, in this case, a simpler way of calculating the source term was employed and found empirically to provide accurate calculated responses in most cases. The procedure is to evaluate the source integral in equations (12), and (13) using the Dirac delta function form, and then proportion this result equally among all eight nodes in the matrix equation for the

finite element containing the source.

The boundary conditions are easily incorporated into the computer model. The homogenous Neumann condition is a natural boundary condition of the Poisson equation. It is satisfied automatically in the finite element formulation when the mesh is teminated (Norrie and de Vries, 1978, p. 188). The inhomogenous Dirchlet condition is not a natural boundary condition, but the finite element formulation derived is still valid when the condition is imposed (Mikjlin and Smolitskiy, 1967, p. 163). It is satisfied by simply not performing the nodal calculation at the appropriate bounding nodes, so that the original calculated potential values remain the same throughout the iteration process.

Another important consideration is the determination of when the solution has converged adequately to be considered valid. Of equal concern is the practical problem of trying to minimize the number of iterations required to solve the very large matrix equation required for this problem. A straightforward "point-of-diminishing-returns" argument is used to determine the optimum point to terminate the iteration process. The following threshold for the maximum residual (equation 23) was adopted:

$$W_{max} \leq (\phi_{max}/10000) \qquad (25)$$

where ϕ_{max} is the maximum value of the surface electric potential at the node nearest the source. The maximum residuals typically

are calculated at or near the sources, and the rest of the residuals are generally proportional to the nodal electric potentials. Therefore, if this condition is met, it would require a large number of additional iterations (perhaps 100, or more) to make a significant change in the calculated surface potentials.

Since an isoparametric element matrix contains 18 independent coefficients compared to eight for the regular hexahedral one, the storage requirements for the global coefficient array is reduced if as many undistorted elements as possible are used. Therefore, both types of elements are included in the computer program. A horizon is determined below which all the elements are undistorted (Figure 2), and included in the input to the program. The minimum number of layers of isoparametric elements needed to adequately approximate the terrain is included in the model. This has been empirically determined to be enough layers so that no element has its vertical dimension reduced to less than one-half of its original undistorted value.

In order to further minimize the memory required for the matrix solution, the matrix coefficients are recalculated as needed in the iteration process. A coefficient array is calculated and stored for only one finite element layer at a time. Testing with small arrays indicate that the method costs only about twice as much as storing the entire array, and yet reduces the memory required to store the coefficients by an order of magnitude or more.

If the nodal calculations are performed in the same order

in each iteration, the result is an initial asymmetry in the over-relaxation potentials which slows the iteration process. Therefore, an alternating direction iterative process was adopted. First, nodal iteration proceeds row by row in each layer starting from an upper corner and finishing on the diagonally opposite lower corner. The next iteration begins where the first stopped and proceeds row by row and layer by layer in precisely the opposite direction. The iterations are alternated in this manner through completion of the solution. This method has been successfully employed by other authors in similar problems (eg., Gunn, 1964).

A complete listing and operating instructions for the computer program have been outlined in detail by Holcombe (1983). The report by Holcombe (1983) also contains verification tests of the modeling program, with comparisons to simple models that have been previously published in the literature.

Computer Model Examples

Computer model responses were generated to illustrate what can be expected from a hole-to-surface resistivity survey for various parameters. The x-y grid used for the finite elements in the models is shown in Figure 6. The finite elements close to the source are small (50 m), while the finite element size is increased away from the source. Computational accuracy is good for the smaller elements close to the source, and decreases away from the source. The effects of decreased accuracy away from the source can be identified by a deteriation of the symmetry of the model response at the outer boundry of the finite element grid.

The effects of varying the following parameters are considered: (1)body size, (2)distance of the source from the body, (3)vertical position of the source with respect to the body, and (4)body shape. These situations are illustrated for resistive and conductive bodies, with deep (500 m, and 700 m) and shallow (100 m) source positions. The electrode configuration consists of a pole source, with a total electric field receiver on the surface. The response with the body present is normalized to the response with the body absent (homogenous halfspace, or layered earth). A normalized response of 1.05 (resistive body) or 0.95 (conductive body) would yield a 5 percent anomaly in the field, which may be detectable. Responses of 1.01, or 0.99, would be below the noise level of normal field measurements and would probably not be detectable.

The effect of varying the body size for a shallow

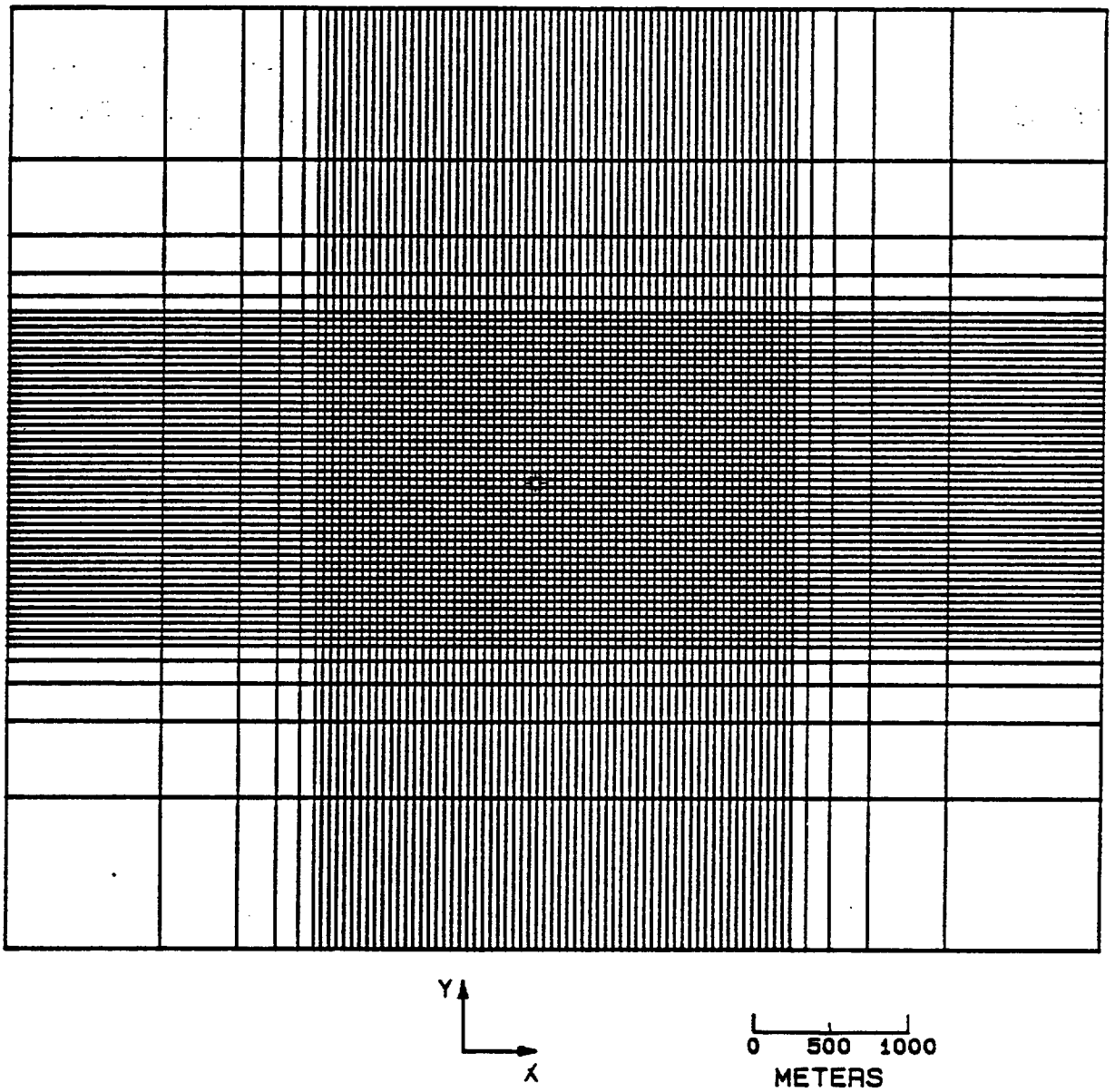

Figure 6. X-Y areal view of grid mesh used to compute the model responses in the examples shown in this paper.

conductive body is shown by comparing Figures 7, 8, and 9. The top of the body and the source depth in these figures are constant. Maximum amplitudes of the anomalies are well within detectability limits, and the size of the anomalies are a function of the size of the bodies. An anomaly associated with a conductive body consists of a resistivity low directly over the body, and an associated resistivity high. The associated resistivity high is often called a "shadow" anomaly. The size and amplitude of the shadow anomaly varies with the proximity of the source to the body, and the intrinsic body parameters (size, depth, and resistivity). A similar correlation between the size of the body and the size of the anomaly can be seen for the models generated using a deep source (Figures 10, 11, and 12). These figures for the deep source also illustrate that the areal size and amplitude of the shadow anomaly is higher for shallower, and larger bodies.

The effect of the distance of the source from the body can be seen by comparing Figures 13, and, 14 with Figures 7, and 8 respectively. There is very little degradation of the anomaly amplitudes for the shallow bodies in Figures 13 and 14, in contrast to the bodies in Figures 7 and 8 that are closer to the source. The size of the anomalies are decreased when the source is further away from the body.

The amplitude and size of the anomaly is strongly dependent upon the depth to the top of the body. This is illustrated in Figures 15, 16, and 17 for the deep source. In general, a deep body results in a broader, lower amplitude anomaly than a shallow body of the same dimensions. The shadow anomaly also becomes

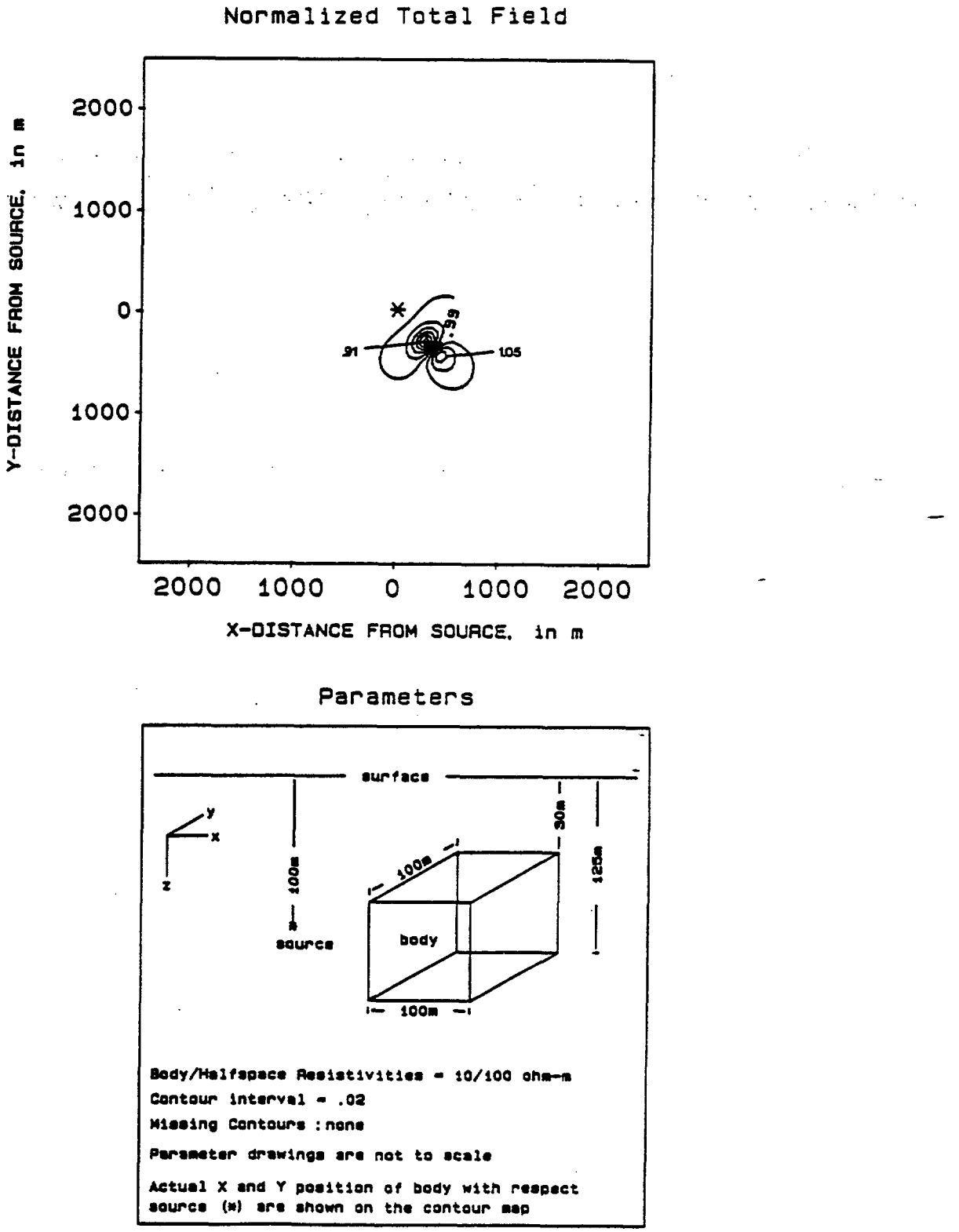

Figure7. Varying the size of a conductive body for a shallow source. Body width is 100 m.

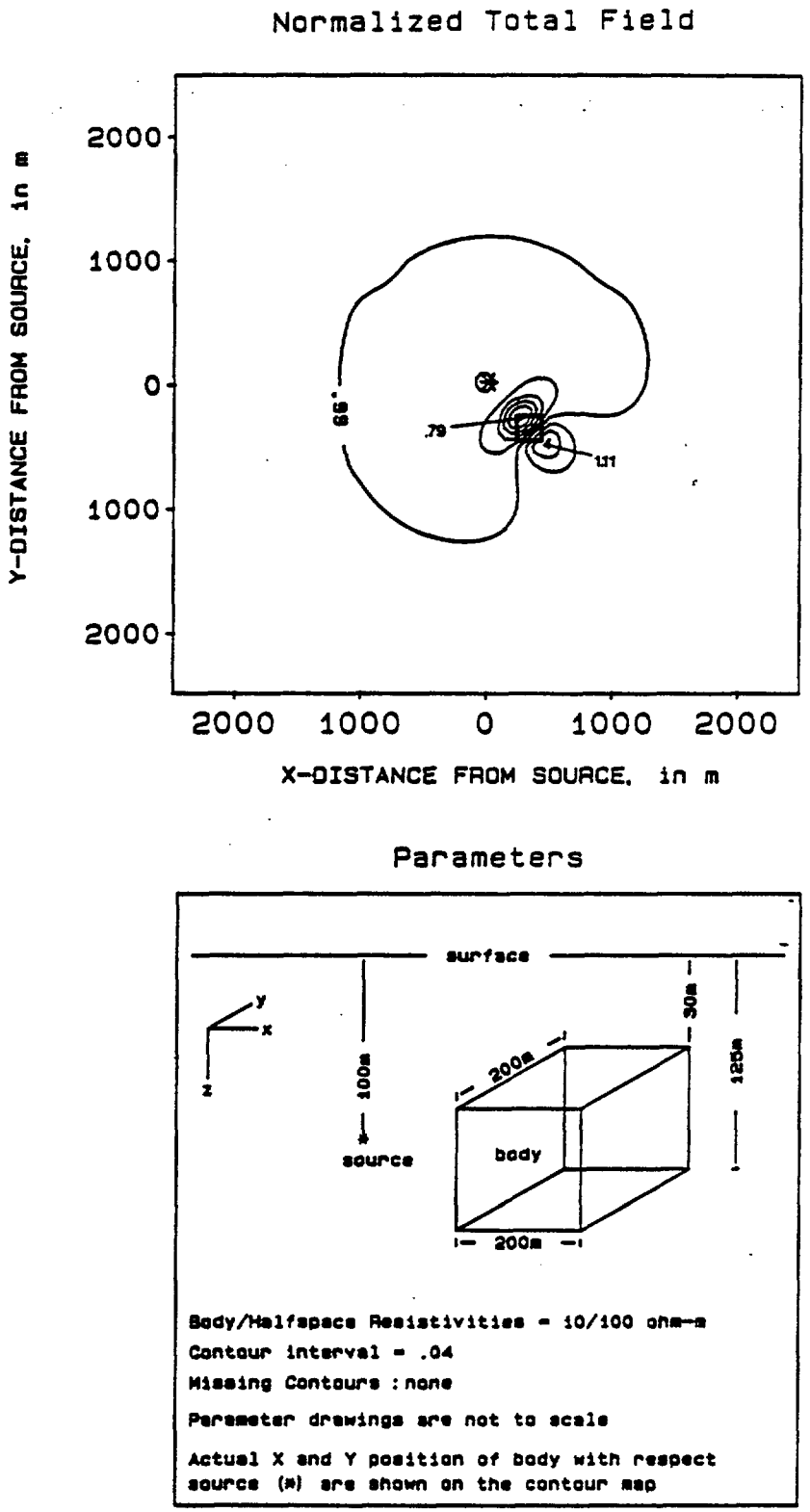

Figure 8. Varying the size of a conductive body for a shallow source. Body width is 200 m.

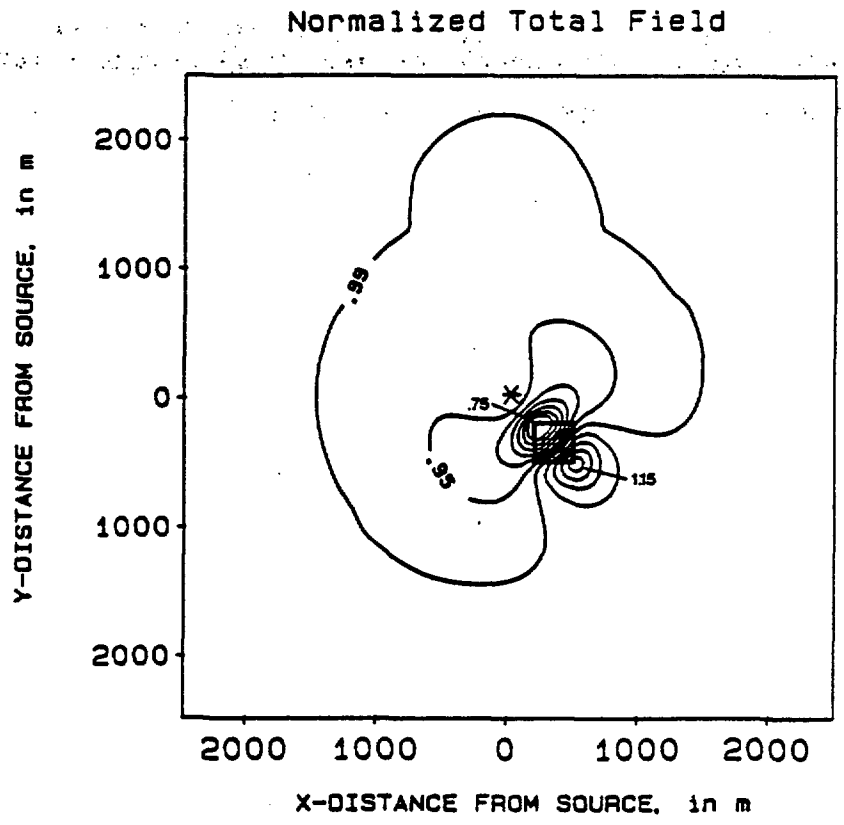

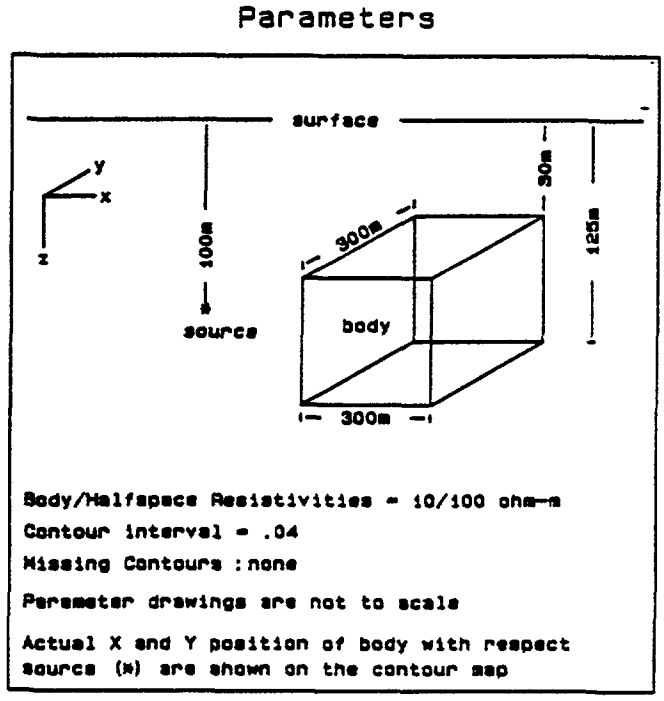

Figure 9. Varying the size of a conductive body for a shallow source. Body width is 300 m.

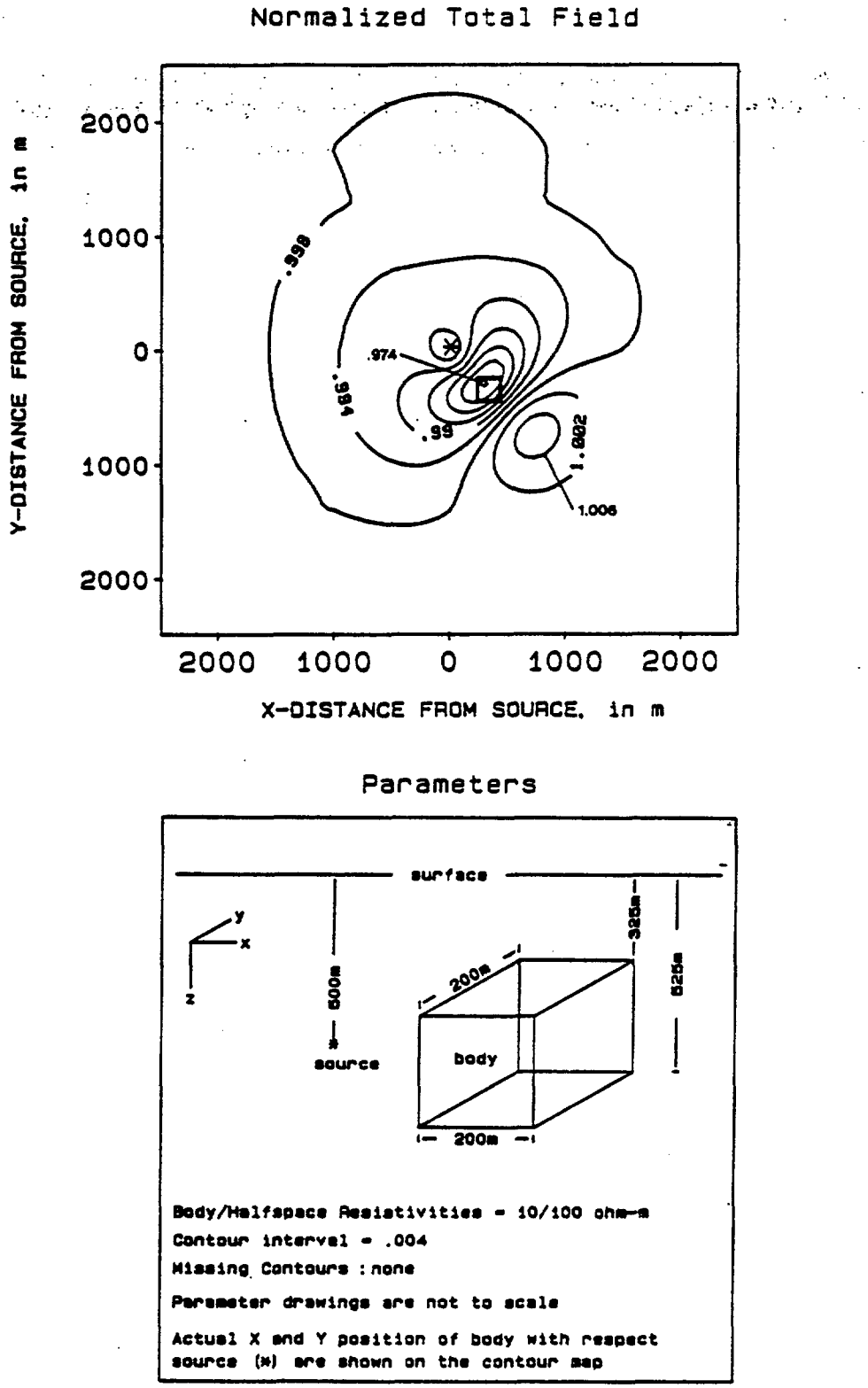

Figure 10. Varying the size of a conductive body for a deep source. Body width is 200 m. Distortion of anomaly in the vicinity of x=0, y=1500 is caused by larger grid size near model boundary.

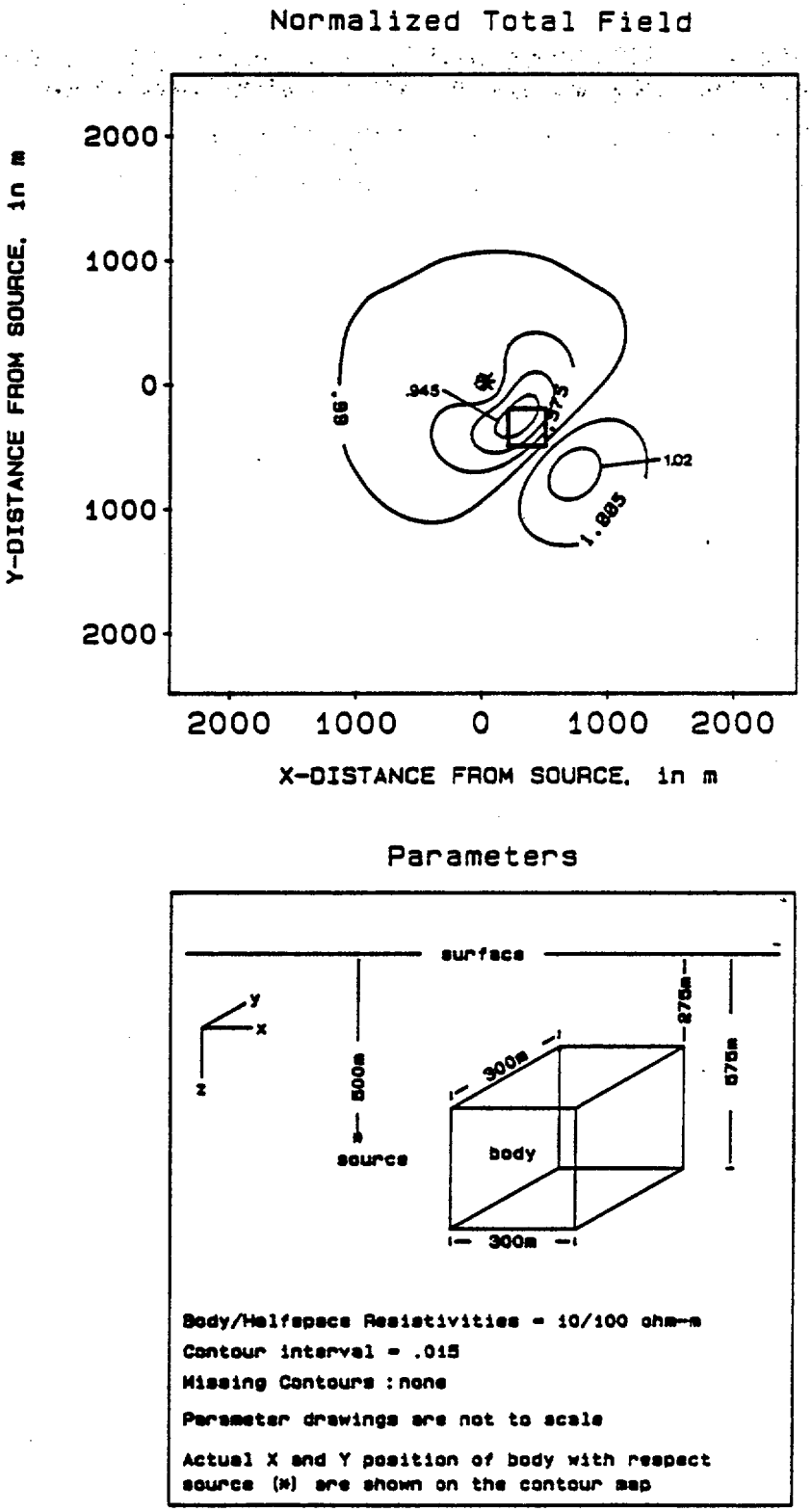

Figure 11. Varying the size of a conductive body for a deep source. Body width is 300 m.

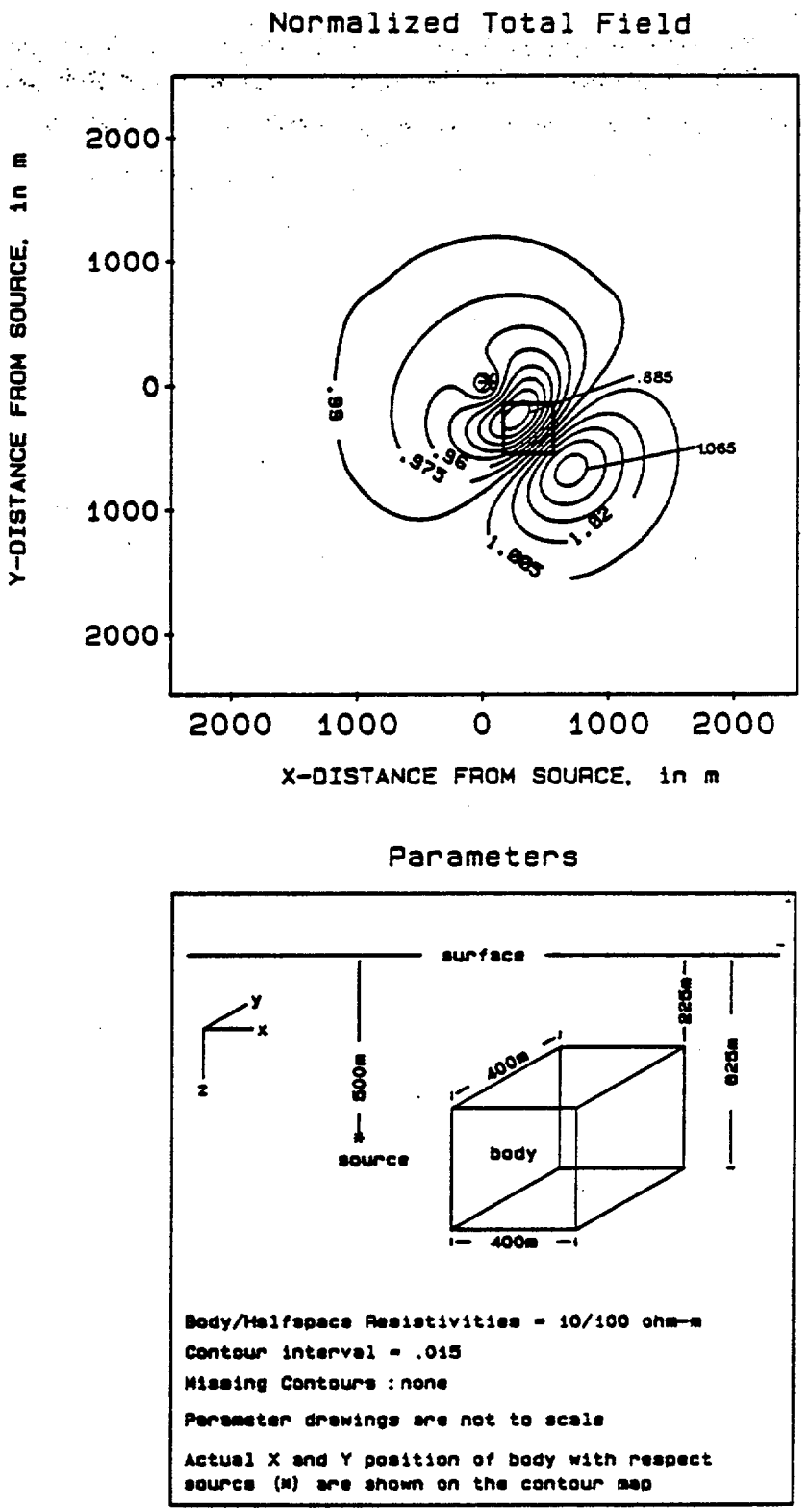

Figure 12. Varying the size of a conductive body for a deep source. Body width is 400 m.

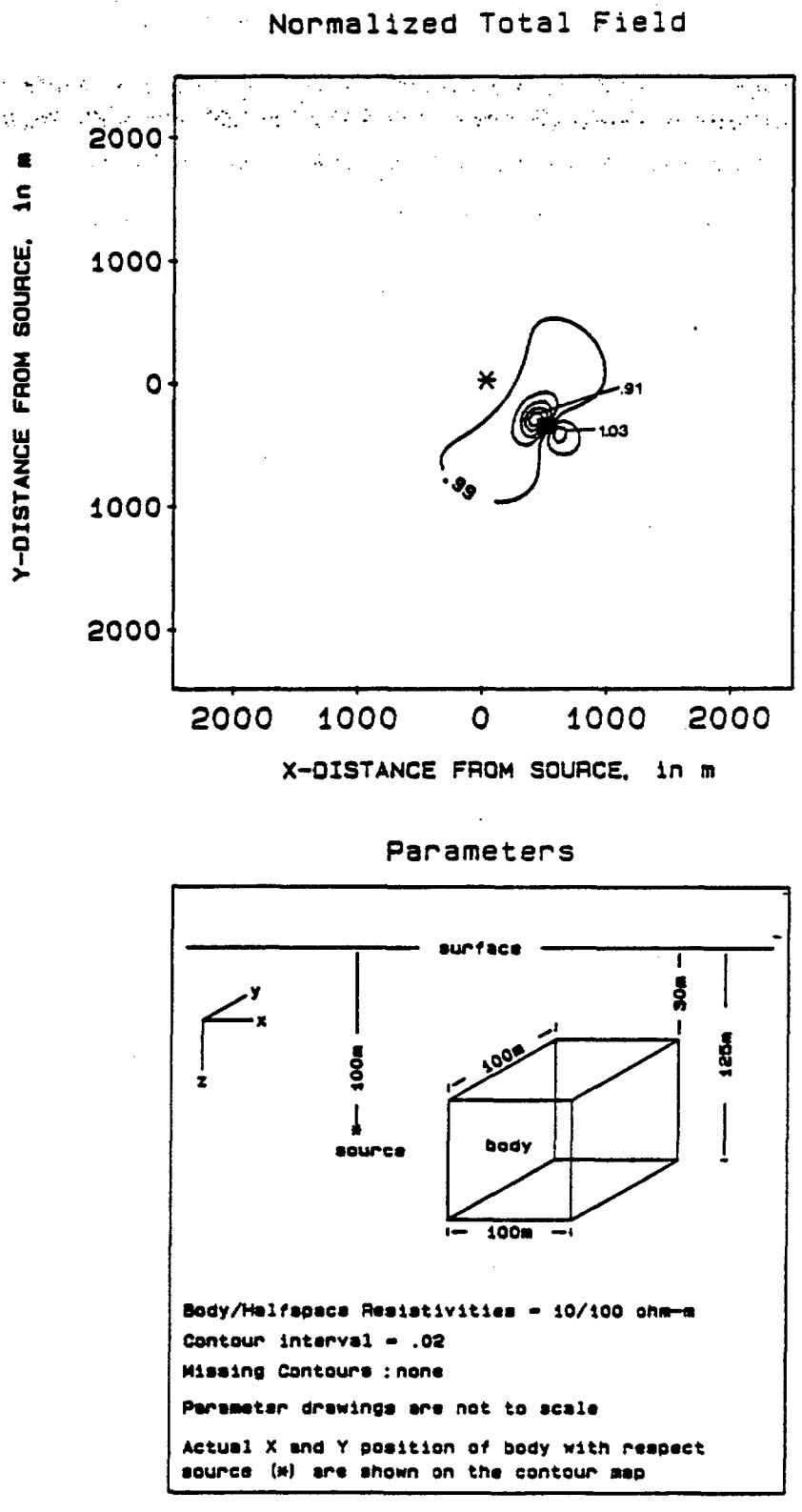

Figure 13. Effect of body distance from the source for a shallow, conductive body further from the source than the model in Figure 7.

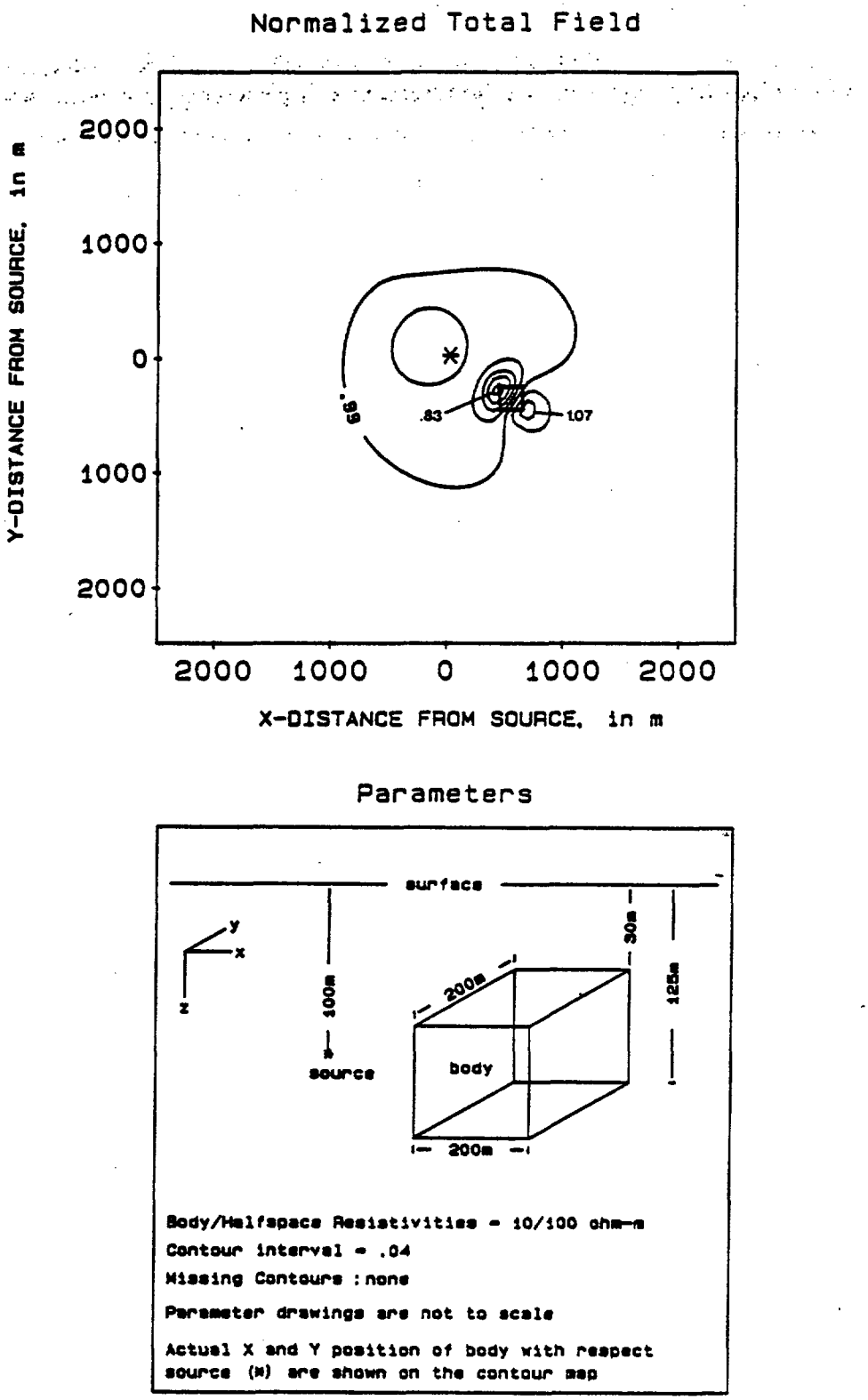

Figure 14. Effect of body distance from the source for a shallow, conductive body further from the source than the model in Figure 8.

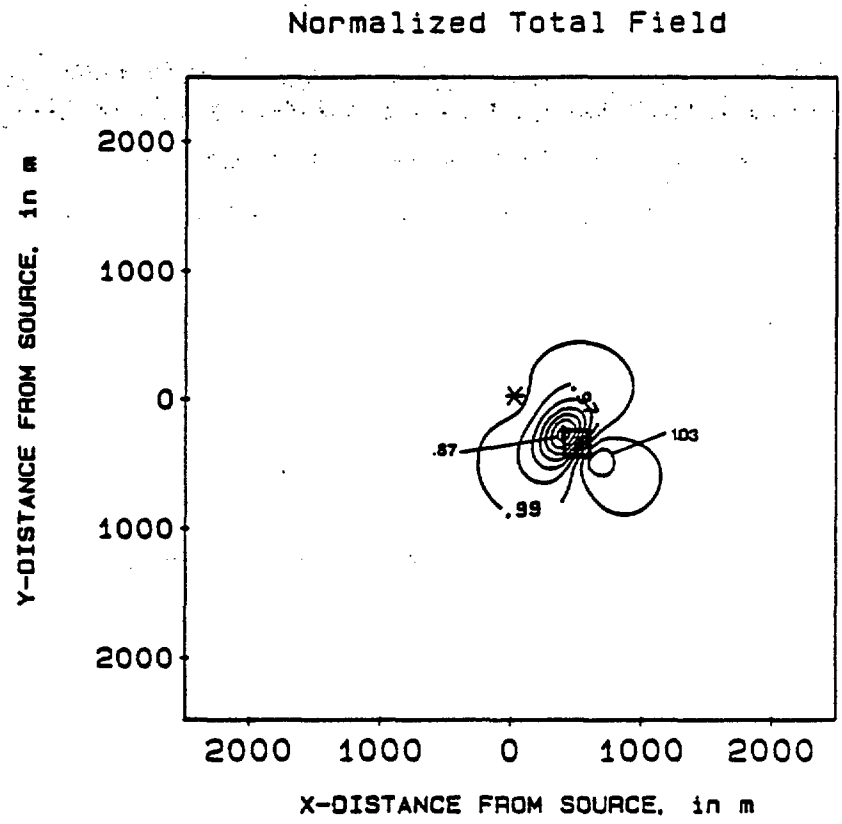

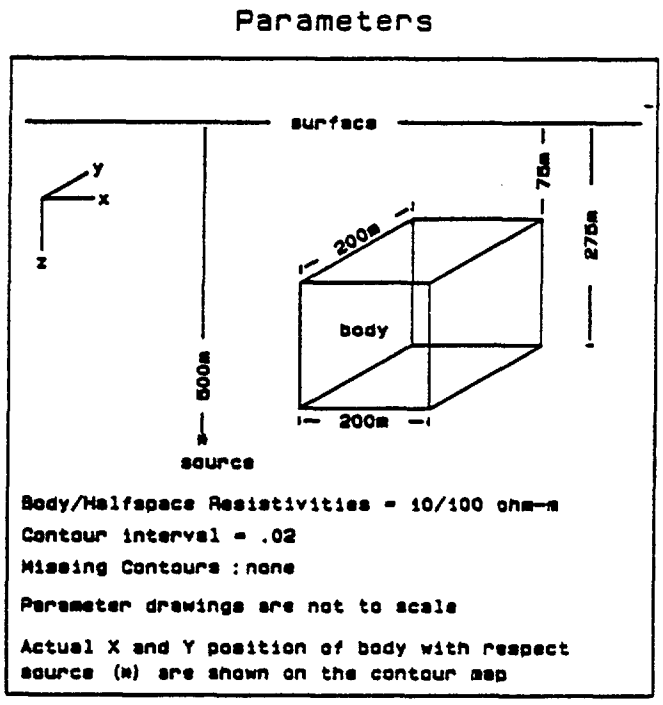

Figure 15. Effect of varying the depth of the top of the body for a conductive body in the presence of a deep source (500 m). Depth to the top of the body is 75 m.

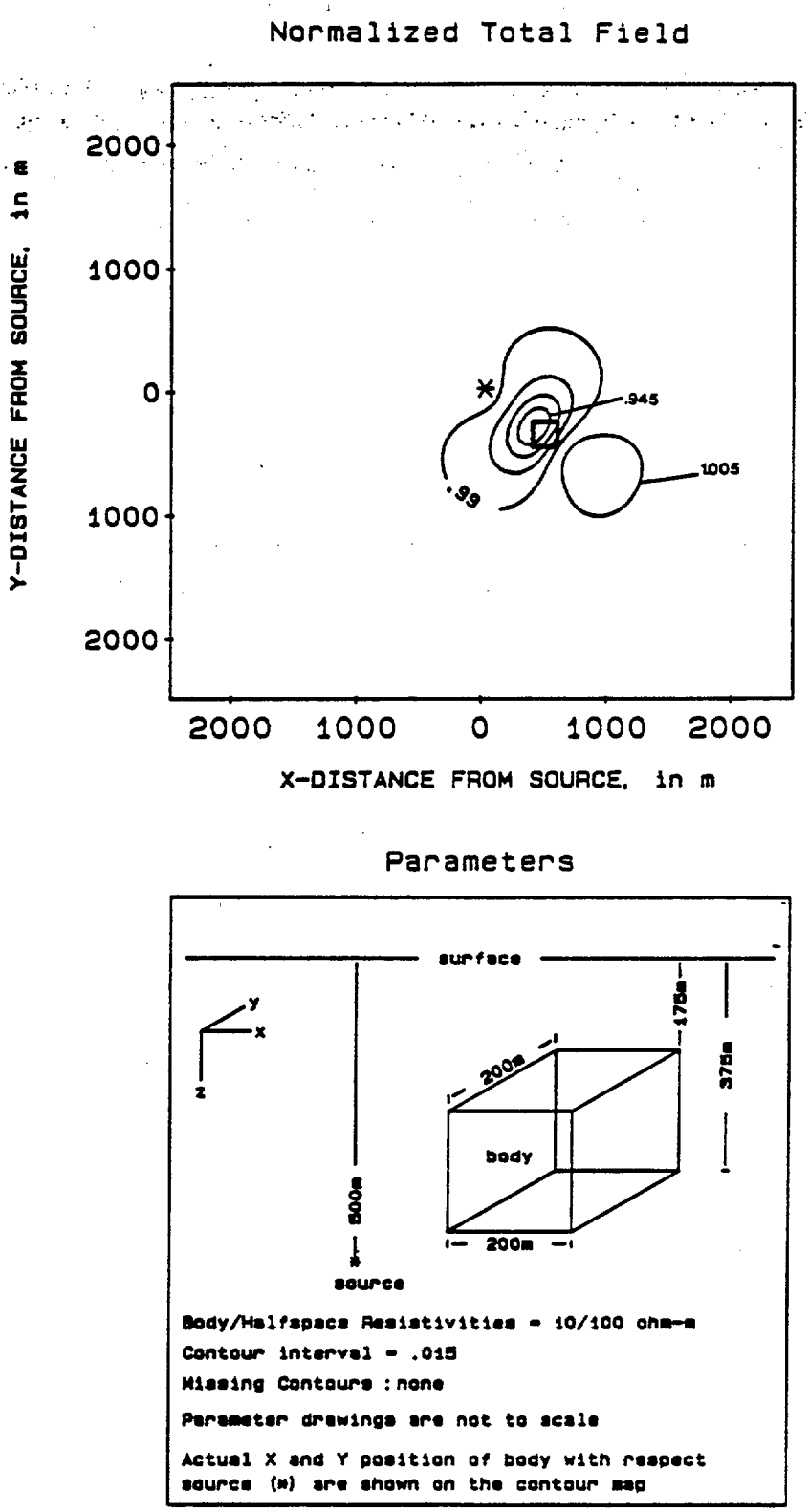

Figure 16. Effect of varying the depth of the top of the body for a conductive body in the presence of a deep source (500 m). Depth to the top of the body is 175 m.

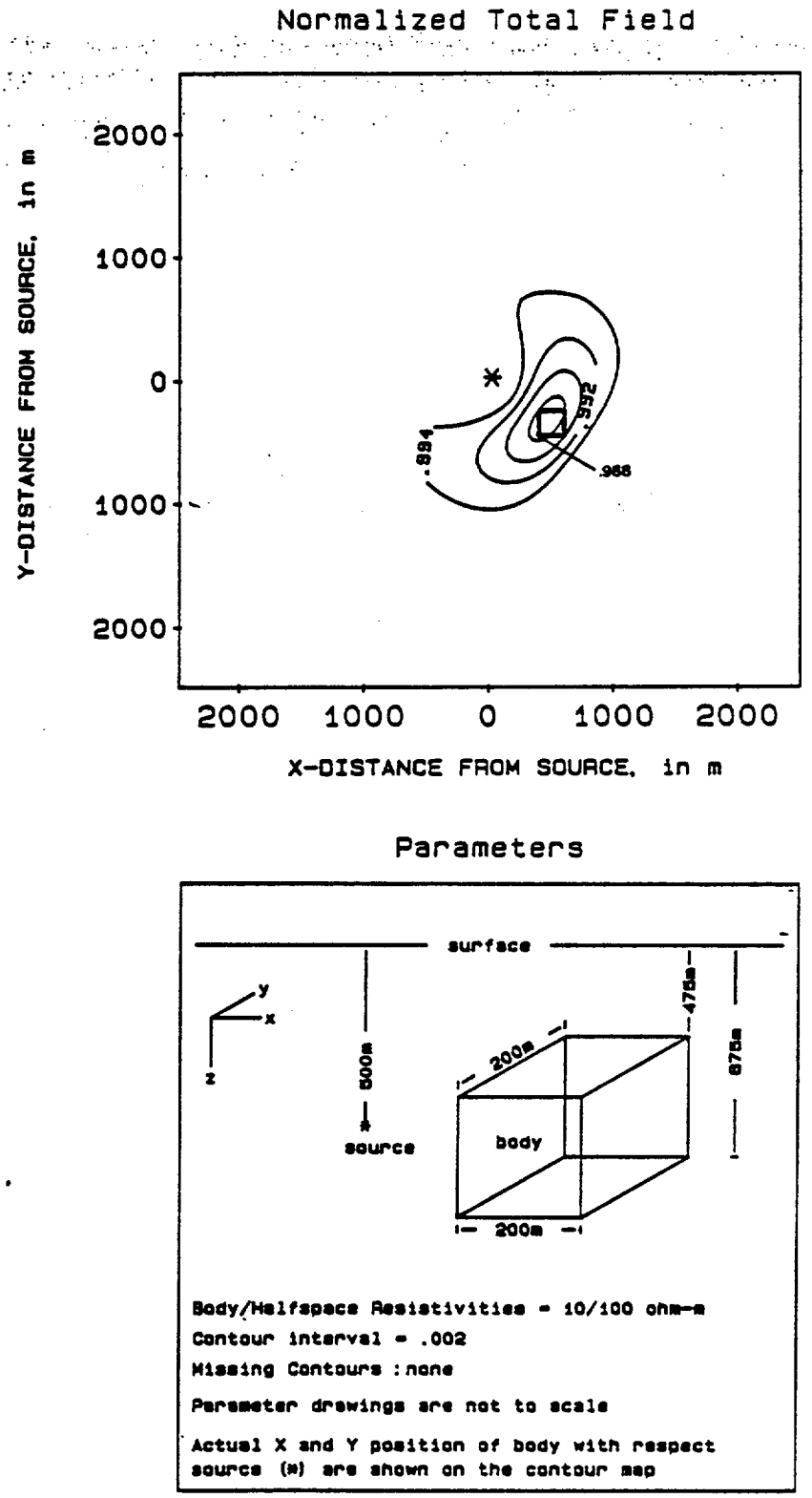

Figure 17. Effect of varying the depth of the top of the body for a conductive body in the presence of a deep source (500 m). Depth to the top of the body is 475 m.

less distinct for a very deep body. However, the shadow anomaly is also a function of the source depth with respect to the body. The anomalies shown in Figures 17 and 18 illustrate responses that are outside the detectability limits of the hole-to-surface resistivity method using a pole source.

The anomalies resulting from resistive bodies of two different lengths are shown in Figures 19 and 20. The length of the anomaly for these shallow bodies is proportional to the length of the bodies, while the maximum amplitude of the anomaly is nearly the same for both bodies. A profile drawn across the body center, and perpendicular to the strike of the body would be nearly identical for the bodies in Figures 19 and 20. Therefore, the body in Figure 19 can be considered to be nearly a two-dimensional body for a profile drawn across its center.

The effect of the vertical position of the body with respect to the source is illustrated in Figures 21, 22, and 23, where the body is below, at the midpoint of, and above the body. It has been previously stated (Daniels, 1977) that the maximum size and amplitude anomaly is obtained when the source is below the body. Figures 21, 22, and 23 reconfirm that the maximum amplitude anomaly for resistive bodies appears to occur when the source is just below the body (Figure 21).

The effect of resistive and conductive noise (in the form of smaller resistive and conductive bodies) on the model response can be seen in Figures 24 and 25. The resistive noise appears to have less of an effect on resolving the square shape of the

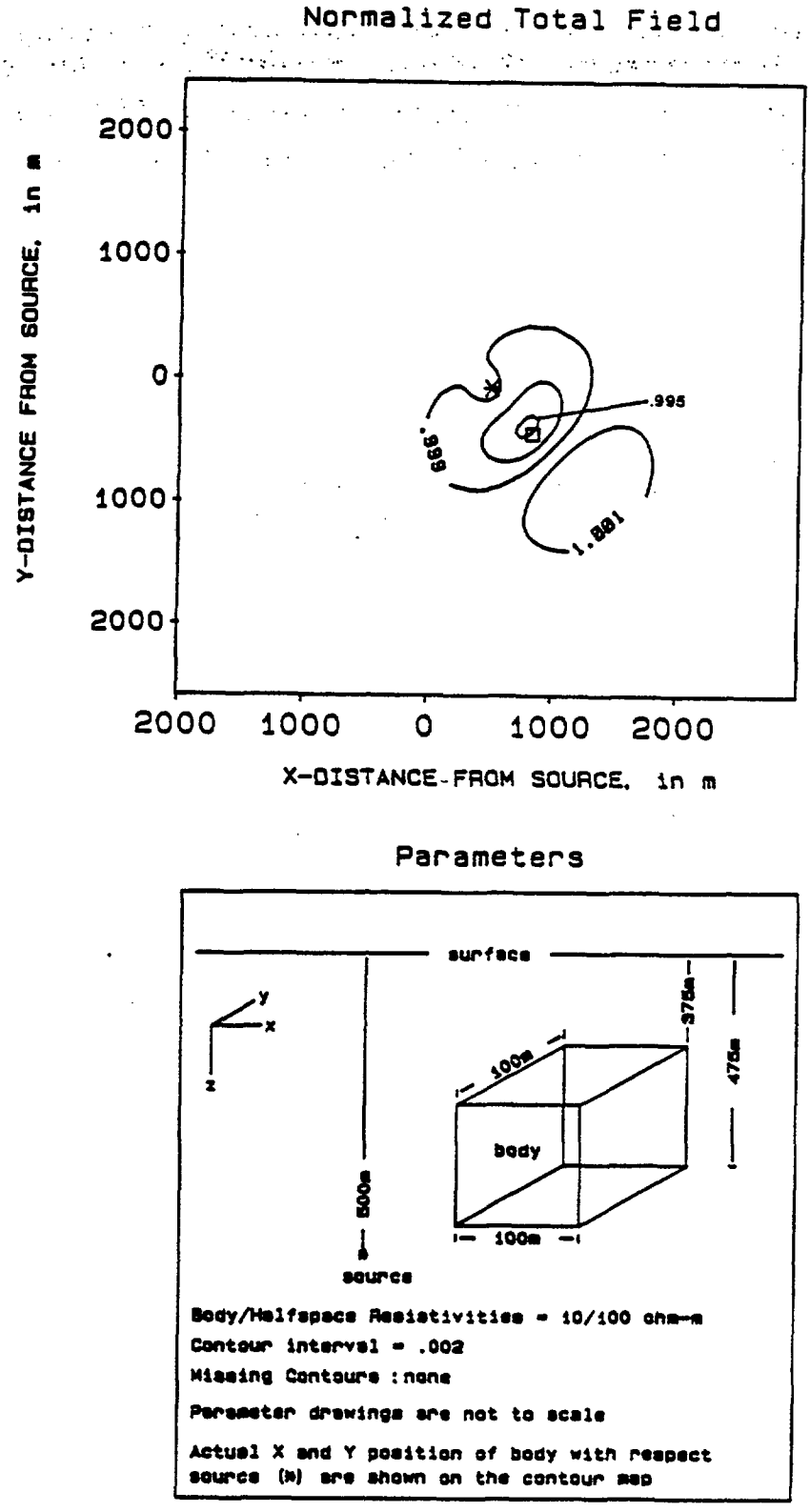

Figure 18. Anomaly with an amplitude that is outside the detectability limits of the hole-to-surface resistivity method.

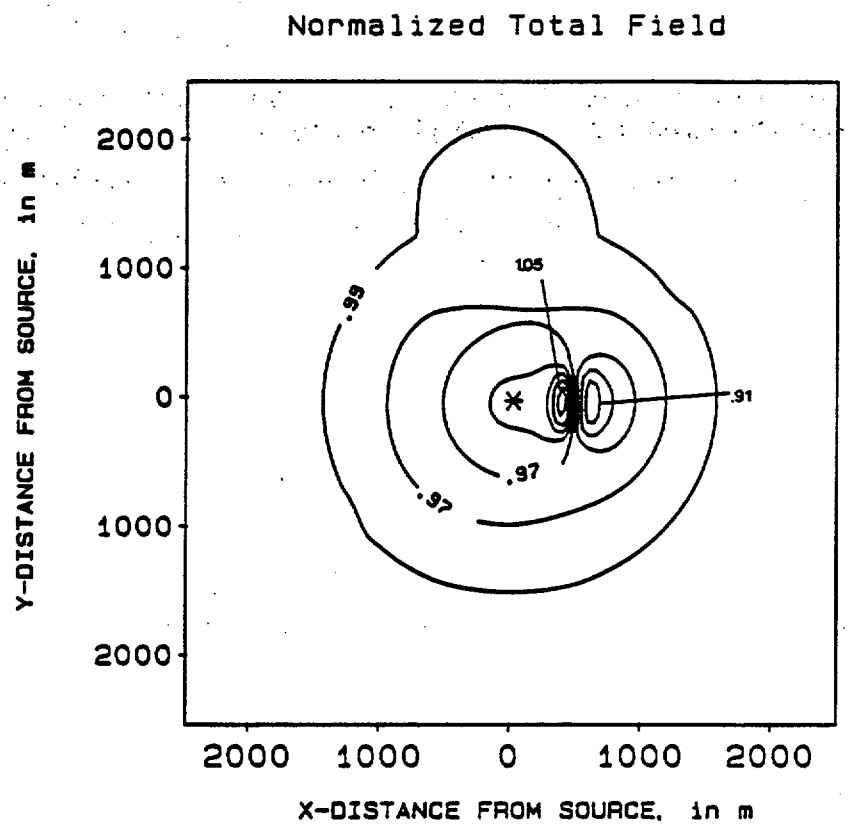

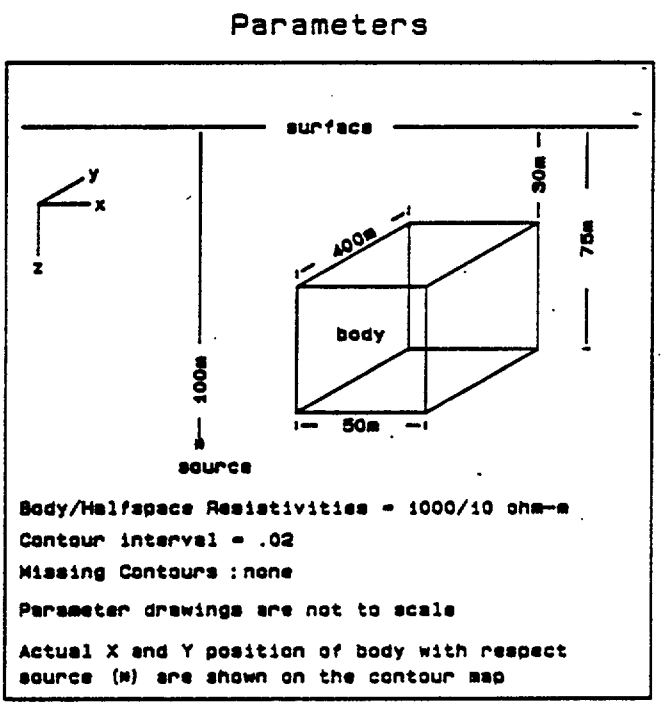

Figure 19. Effect of varying the length of a resistive body on the resistivity response. Length of the body is 400 m. Distortion of anomaly in the vicinity of x=0, y=1500 is caused by larger grid size near the boundary of the model.

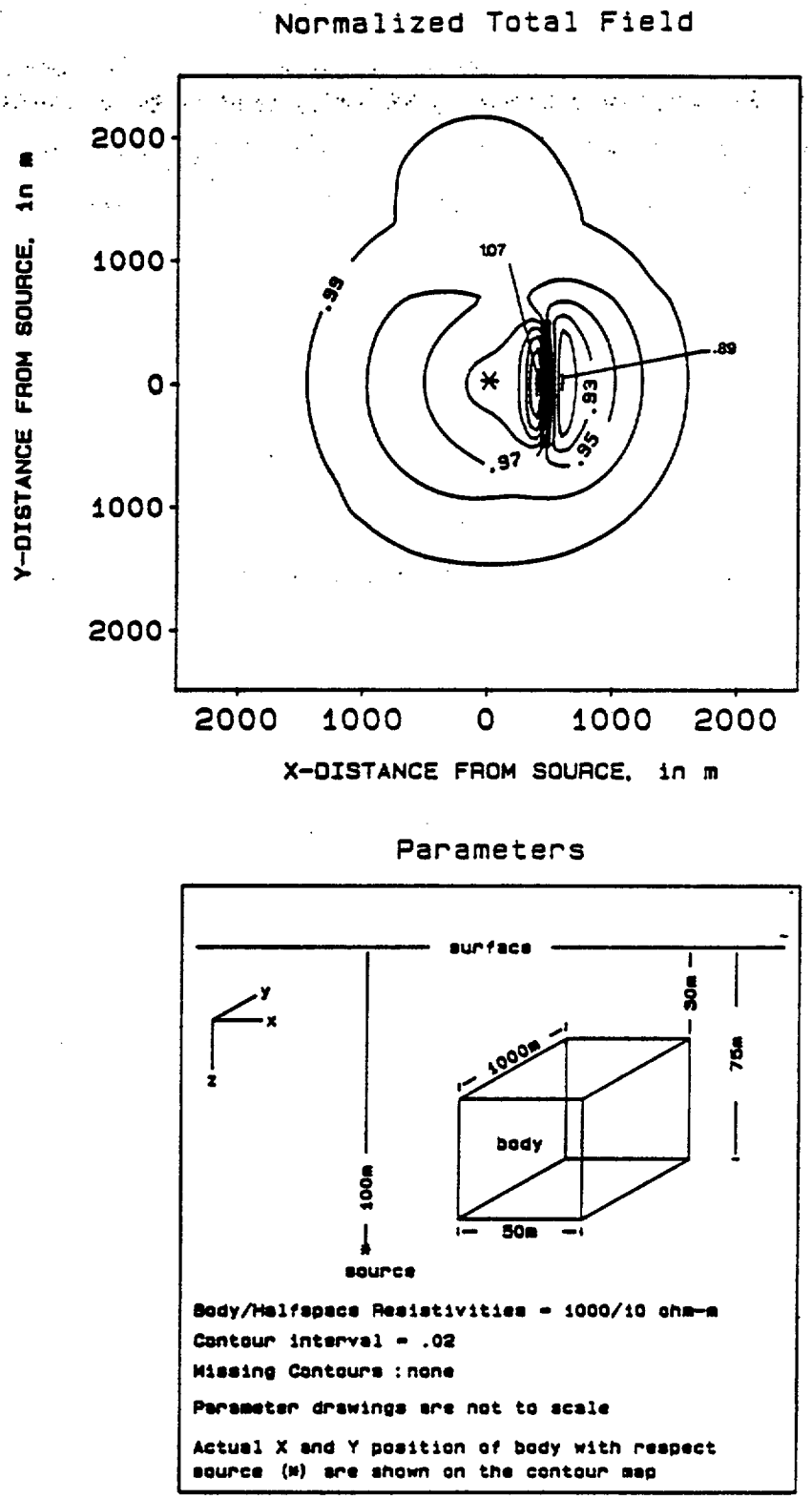

Figure 20. Effect of varying the length of a resistive body on the resistivity response. Length of the body is 1000 m. Distortion of anomaly in the vicinity of x=0, y=1500 is caused by larger grid size near the boundary of the model.

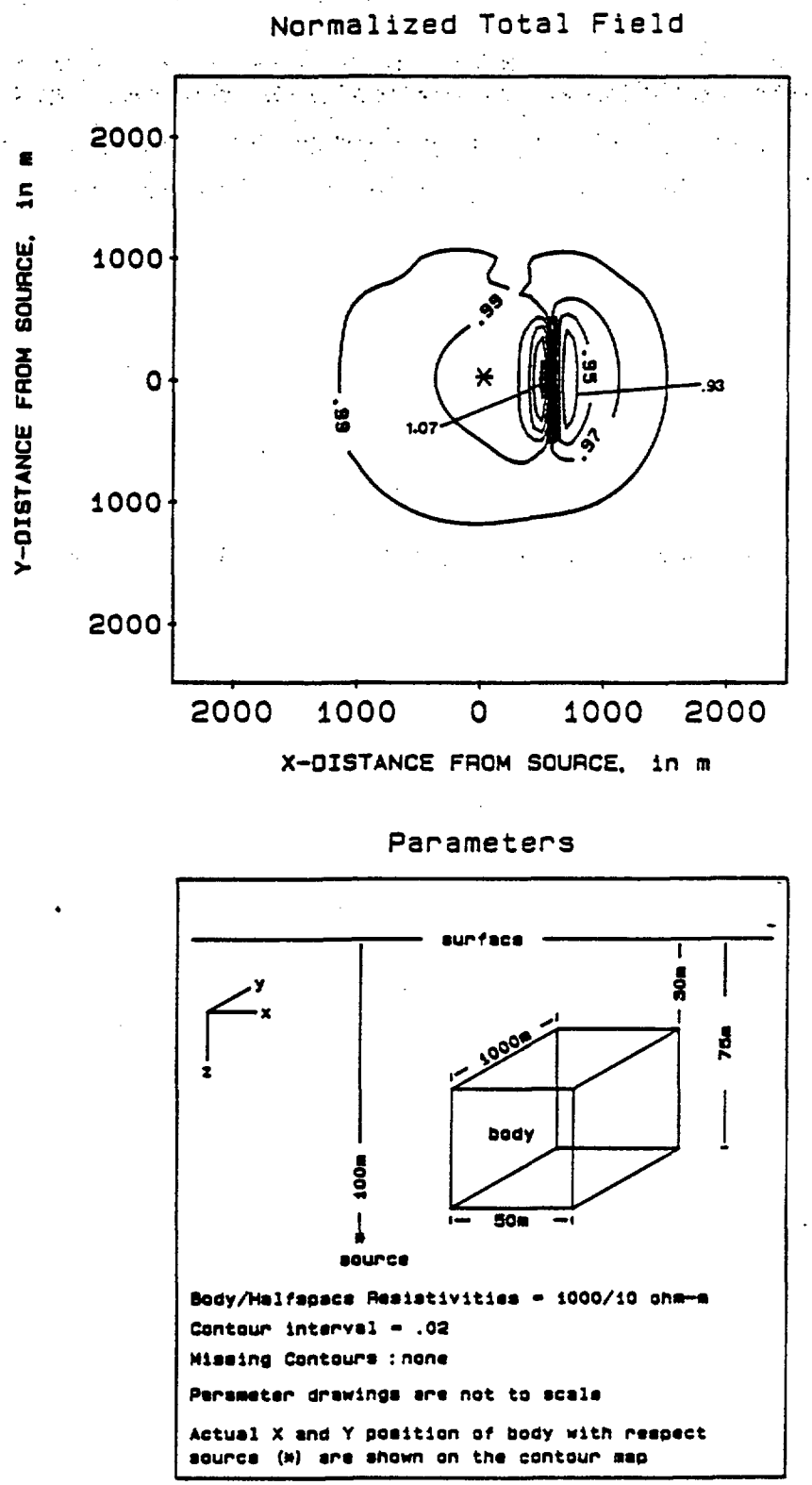

Figure 21. Effect of the relative vertical position of the source. Source below the body.

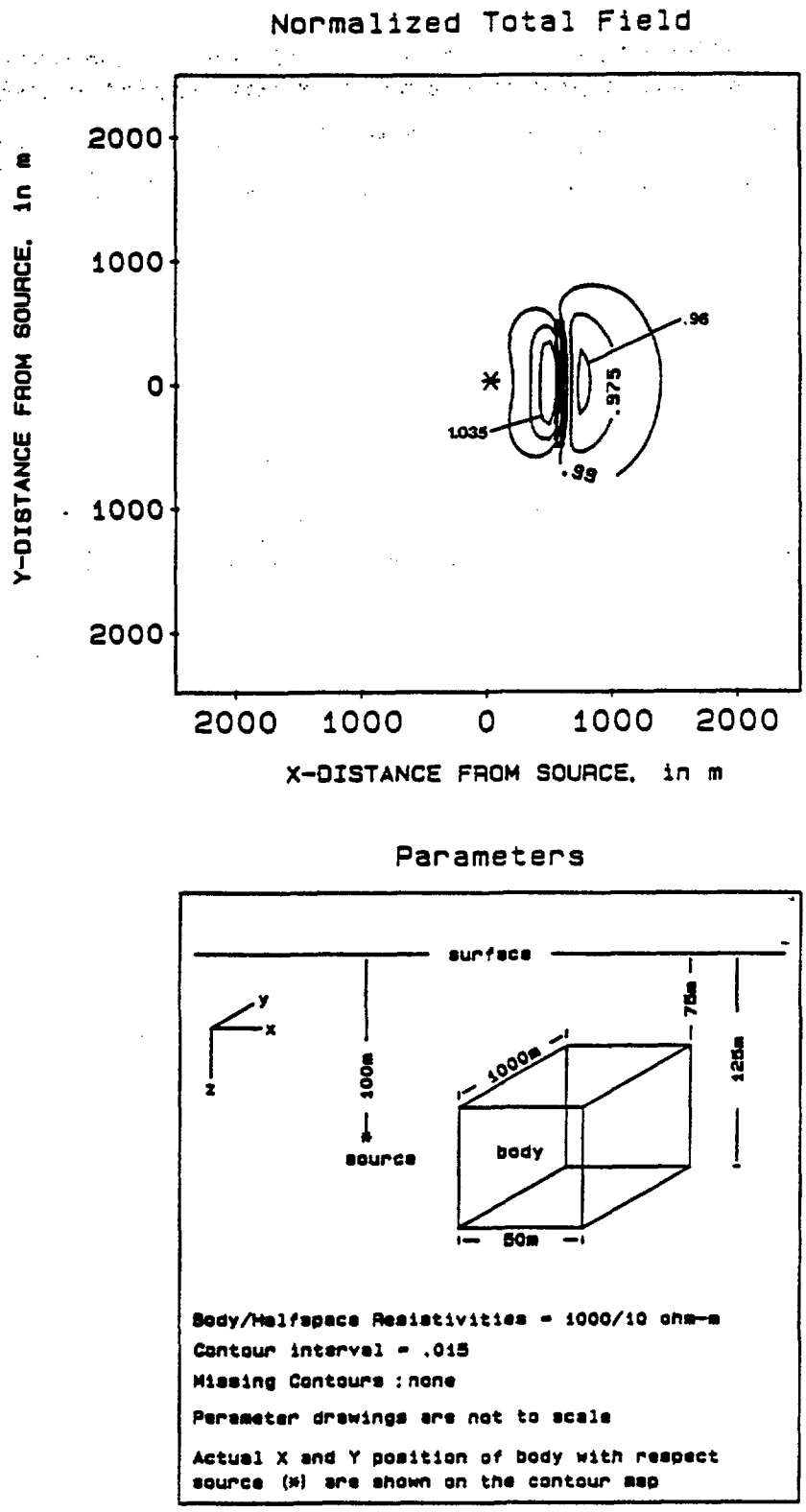

Figure 22. Effect of the relative vertical position of the source. Source depth at the midpoint of the body.

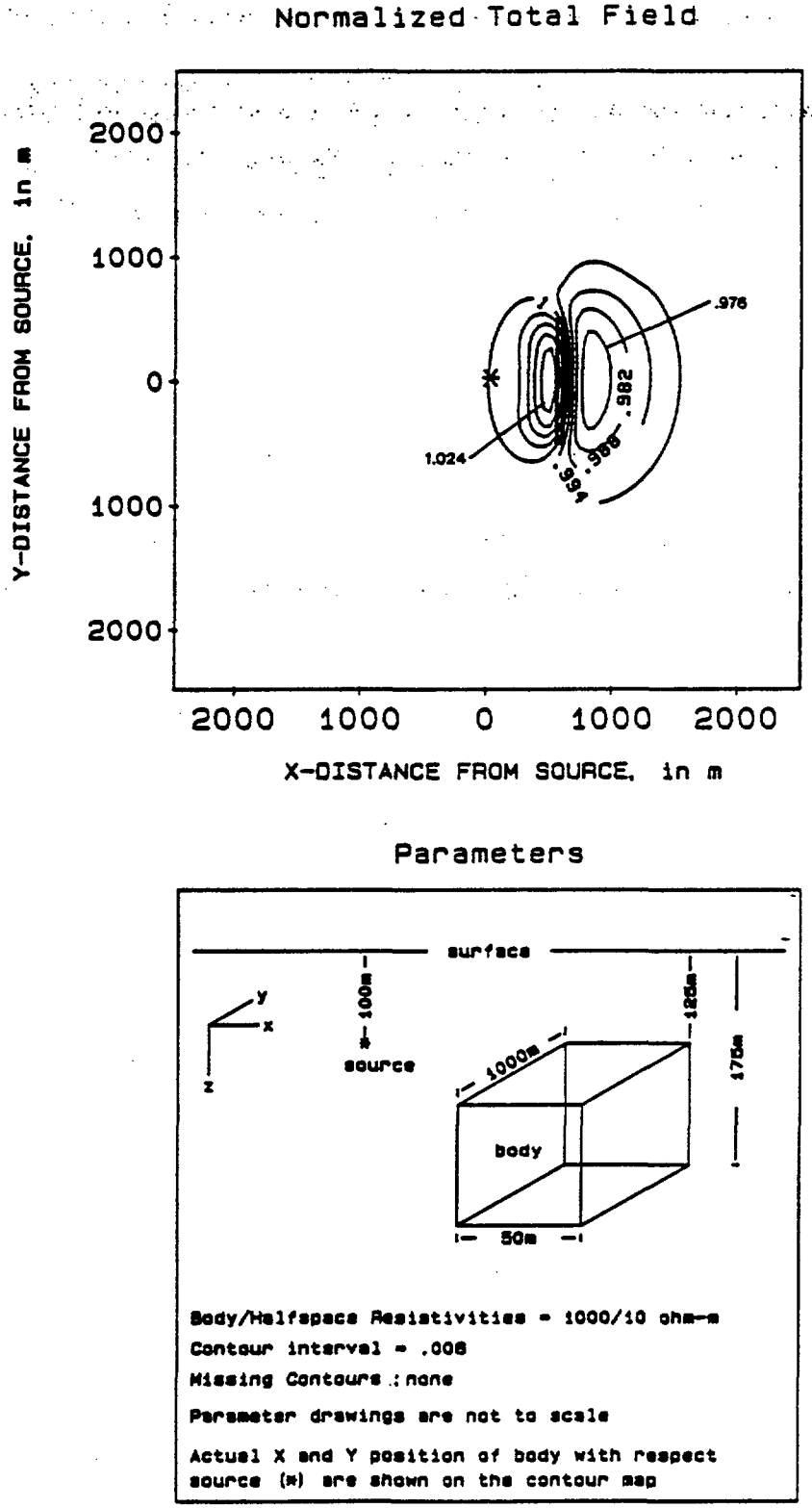

Figure 23. Effect of the relative vertical position of the source. Source above the body.

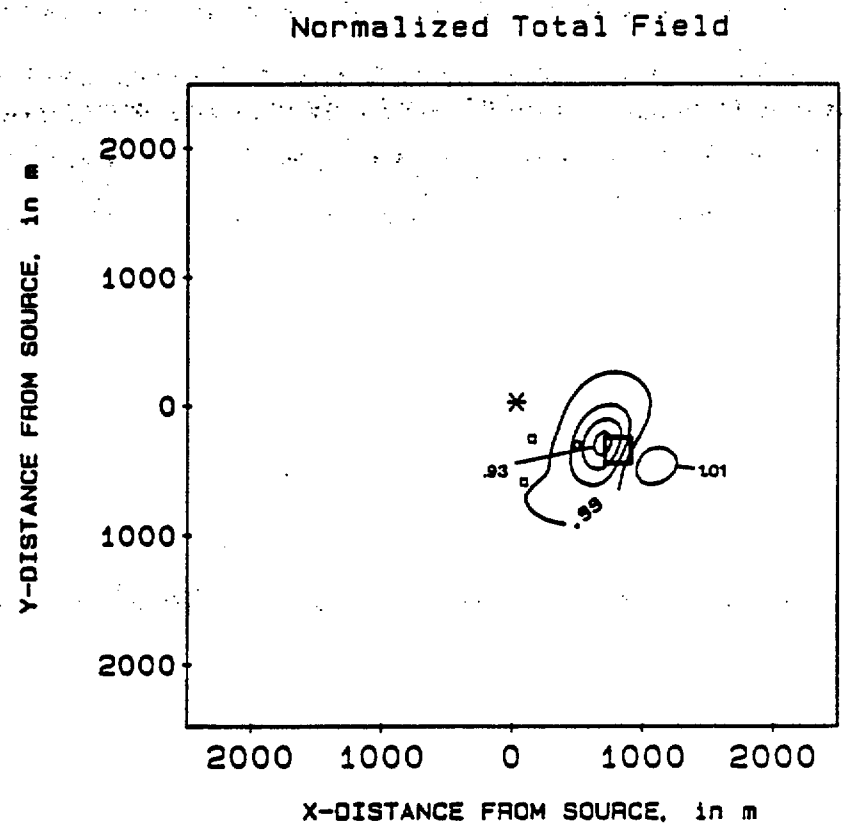

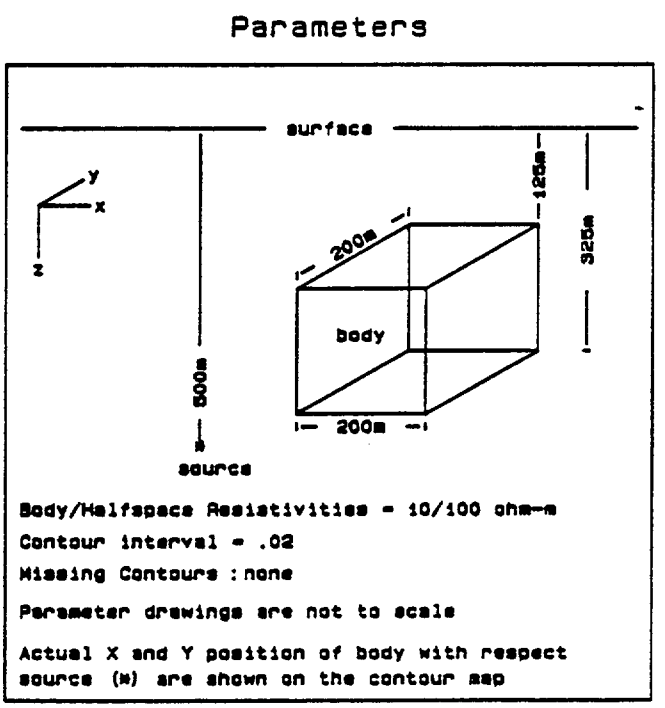

Figure 24. The response of a conductive body in the presence of resistive noise. Resistive noise is simulated by small resistive bodies.

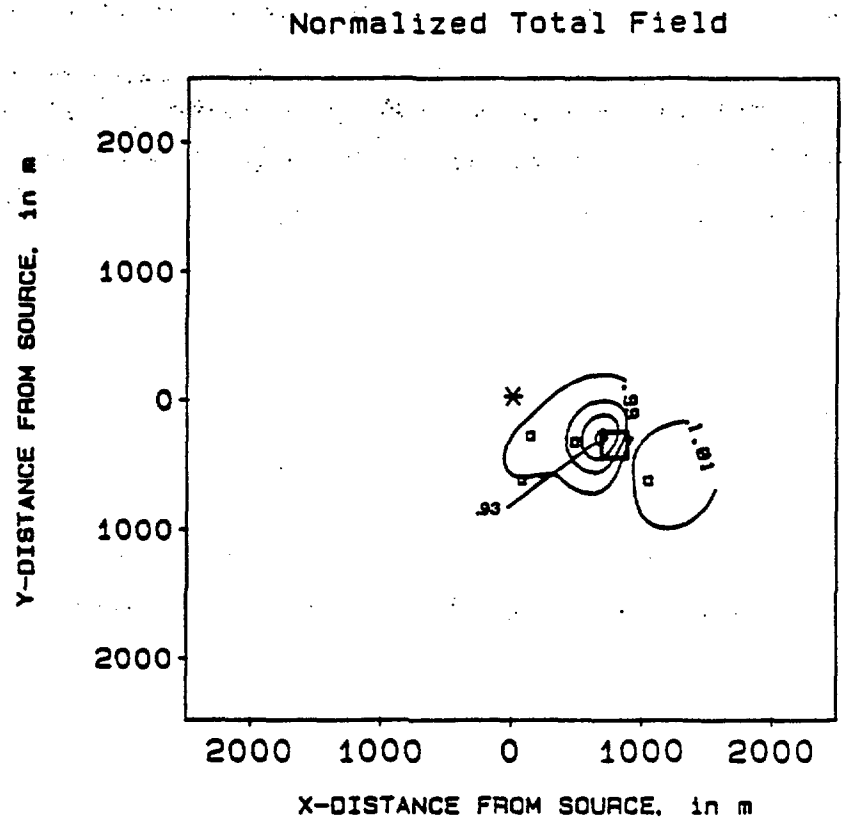

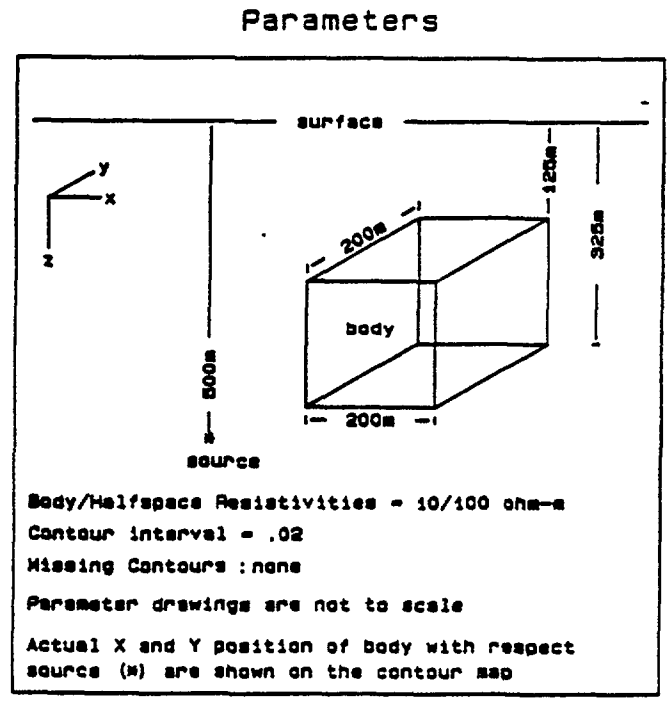

Figure 25. The response of a conductive body in the presence of conductive noise. Conductive noise is simulated by small conductive bodies.

conductive body (Figure 24) than the conductive noise (Figure 25). The amplitude of the main anomalies in both cases are nearly unaffected by the presence of the interfering bodies.

Extremely high amplitude anomalies are seen for the simulated fracture zone (conductive) contained within a deeply buried resistive layer (Figures 26, 27, 28, and 29). These models are directly applicable to hazardous waste sites. The anomalous response for all of the bodies are 20 to 30 percent above the response that would be obtained with the fracture zone absent from the model. Unfortunately, the model responses in Figures 27, and 29 also illustrate the limits of the finite element model for the chosen parameters. The anomalies in both cases should be nearly symmetrical in both the x-, and y-directions. The model responses are valid near the center of the grid, and could be made more accurate near the grid edge by increasing the number of small grid elements near the grid boundry.

Conclusions

The finite element computer model developed for simulating the resistivity response from an arbitrary distribution of subsurface resistivities provides an excellent means of predicitng the detectability of anomolous bodies that might be encountered in hazardous waste site evaluation. Examples for the hole-to-surface resistivity measurements illustrate that both the source position and the body depth and dimensions are important considerations in determining if an anomolous body can be detected by hole-to-surface resistivity measurements. Therefore,

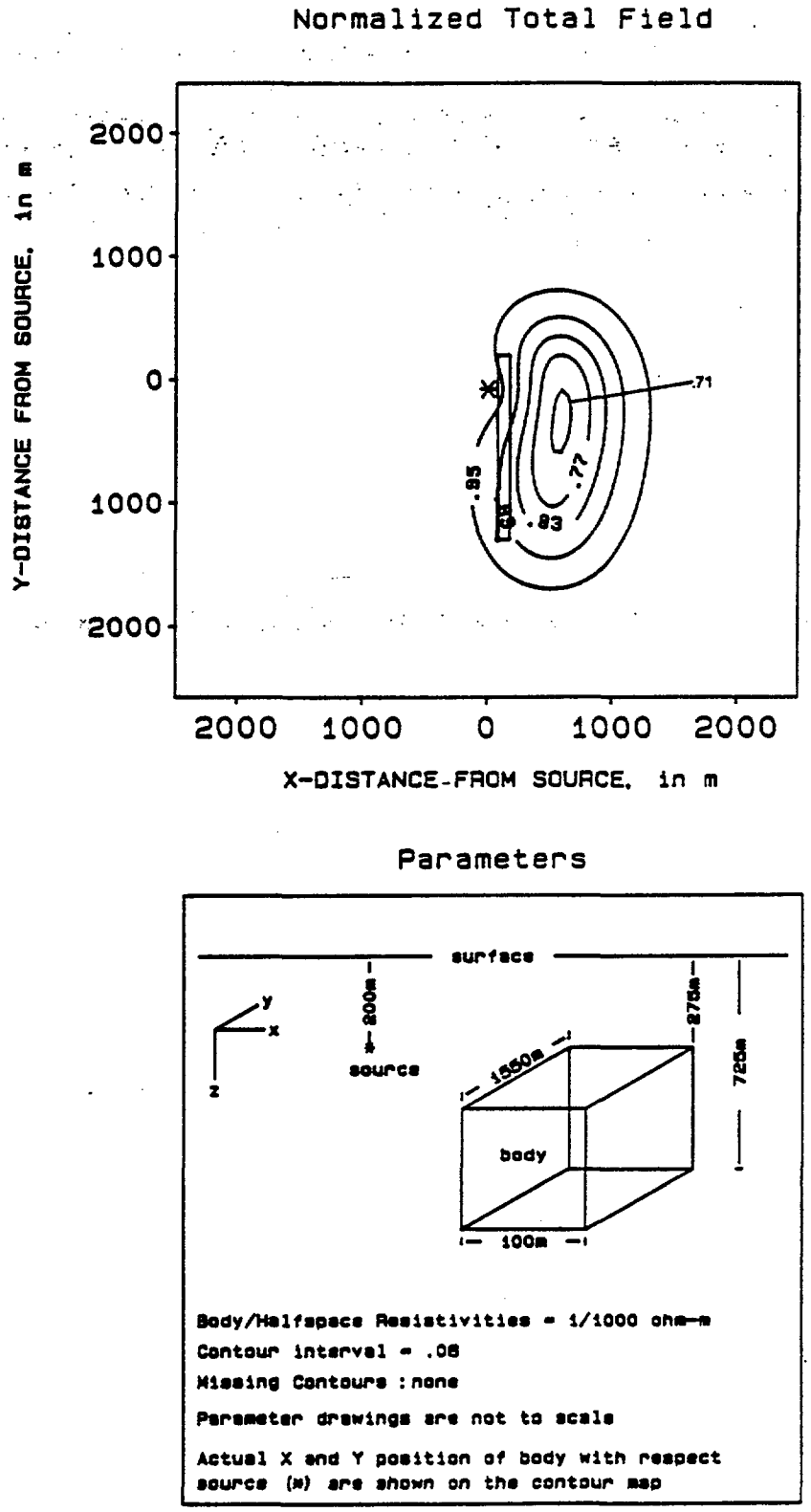

Figure 26. Conductive body contained in a resistive (intermediate) layer of a three-layer model. Resistivity and thicknesses of upper (1), intermediate (2) and lower (3) layers are: (1)20 ohm-m and 275 m, (2)1000 ohm-m and 450 m, and (3) 50 ohm-m and model bottom. Source at 200 m.

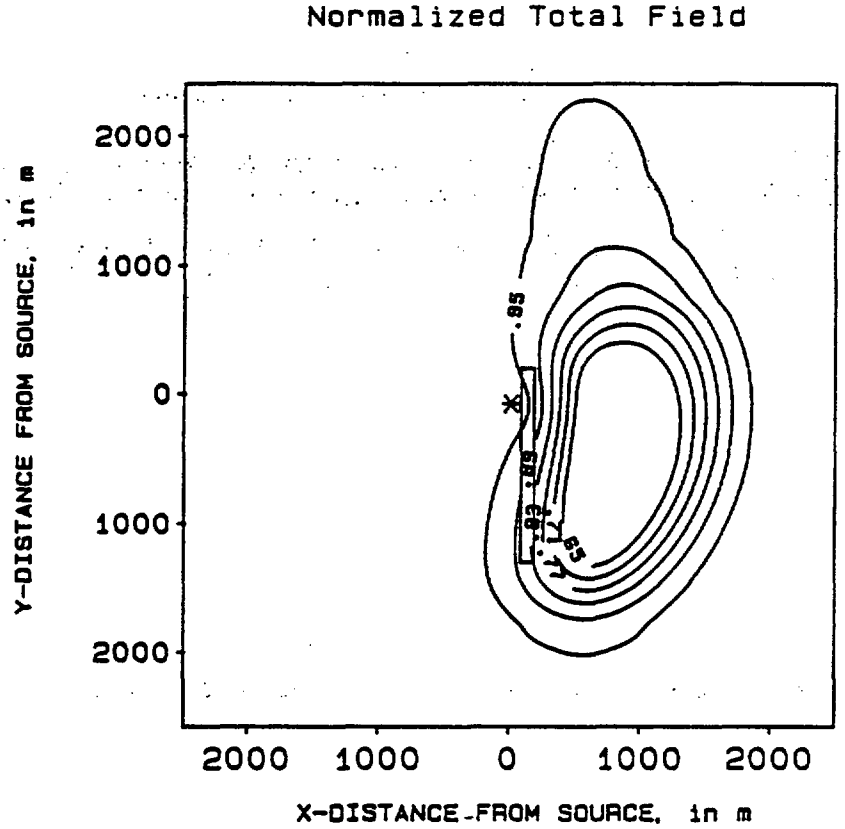

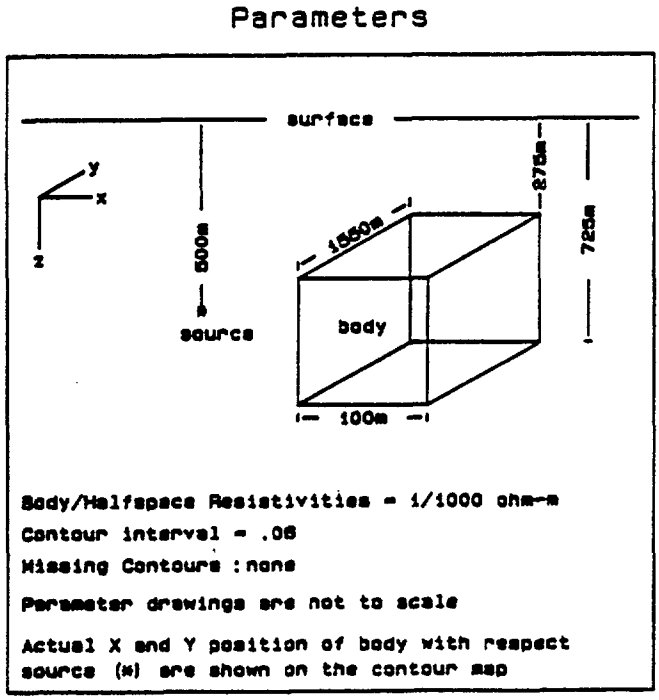

Figure 27. Conductive body contained in a resistive (intermediate) layer of a three-layer model. Resistivity and thicknesses of upper (1), intermediate (2) and lower (3) layers are: (1)20 ohm-m and 275 m, (2)1000 ohm-m and 450 m, and (3) 50 ohm-m and model bottom. Source at 500 m. Distortion of anomaly in the vicinity of x=500, y=1500 is caused by larger grid size near the boundary of the model.

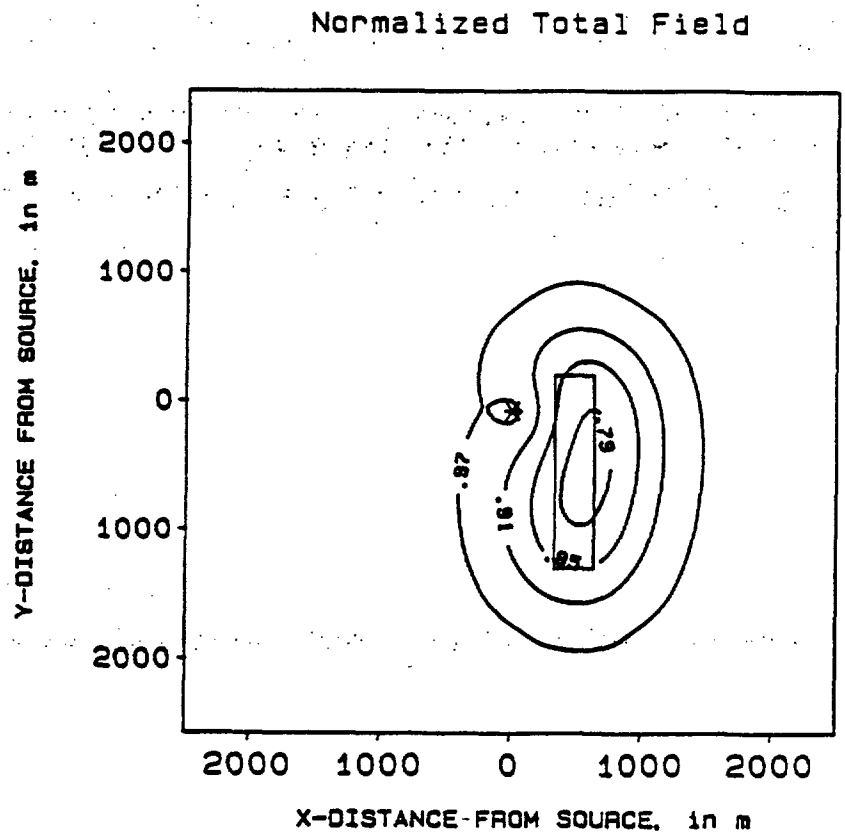

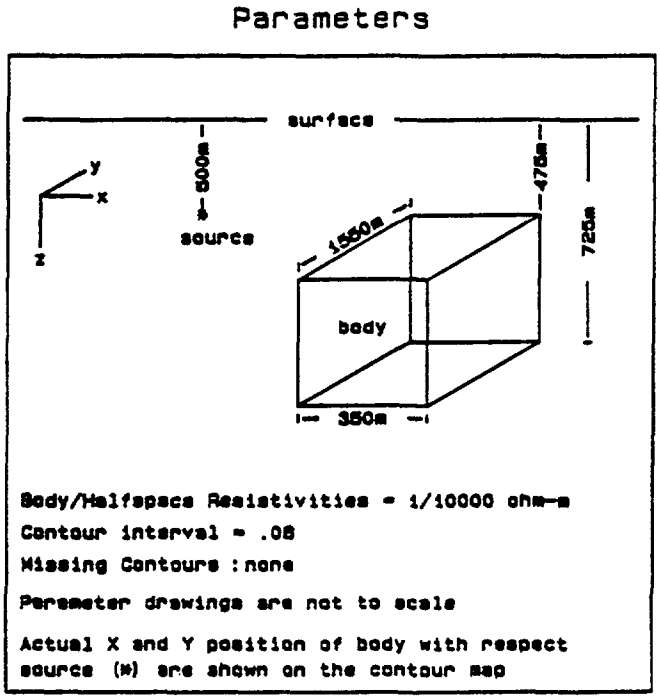

Figure 28. Conductive body contained in a resistive (intermediate) layer of a three-layer model. Resistivity and thicknesses of upper (1), intermediate (2) and lower (3) layers are: (1)20 ohm-m and 525 m, (2)10000 ohm-m and 200 m, and (3) 50 ohm-m and model bottom. Source at 500 m.

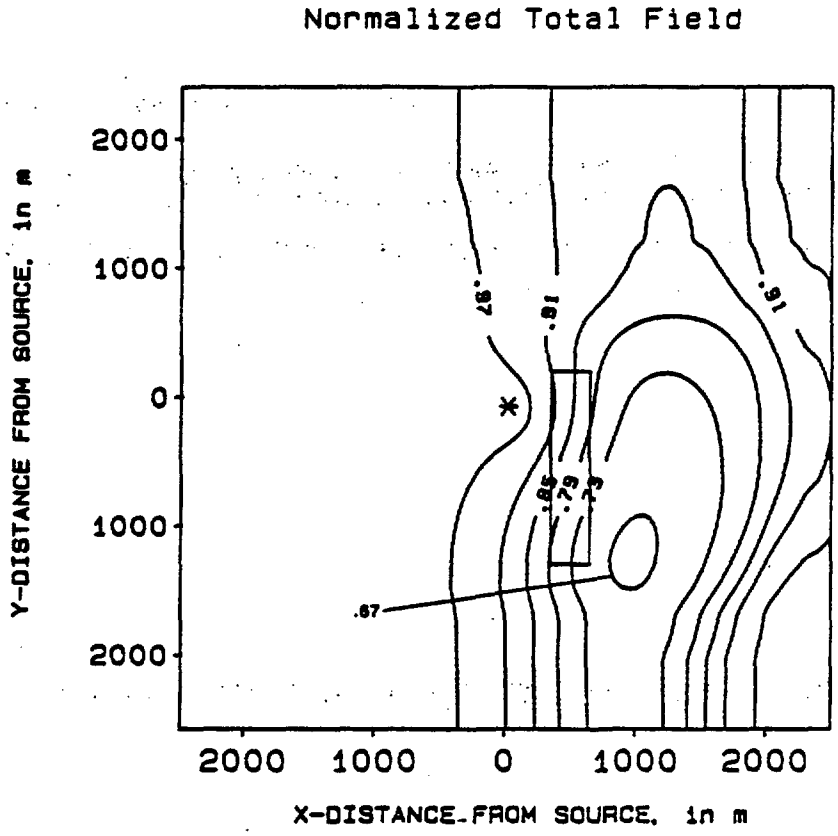

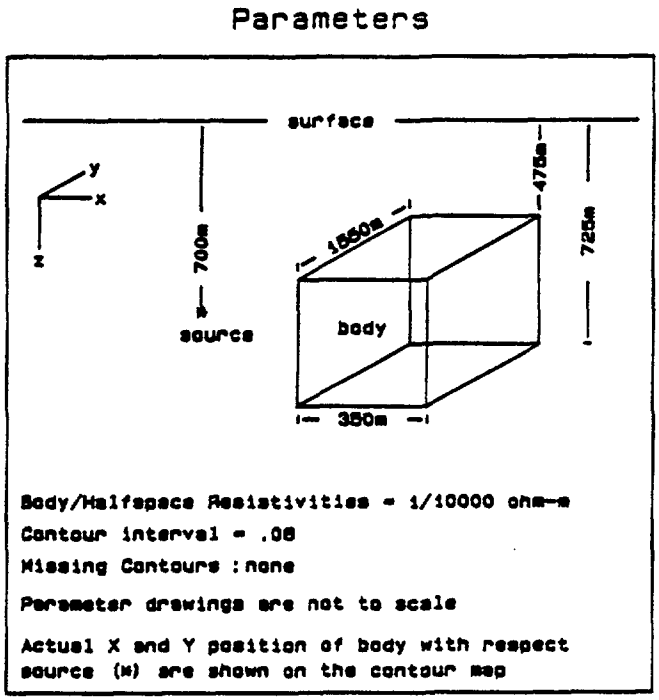

Figure 29. Conductive body contained in a resistive (intermediate) layer of a three-layer model. Resistivity and thicknesses of upper (1), intermediate (2) and lower (3) layers are: (1)20 ohm-m and 525 m, (2)10000 ohm-m and 200 m, and (3) 50 ohm-m and model bottom. Source at 700 m. Distortion of anomaly in the approximate vicinity of y-values greater than 1500 m is caused by larger grid size near the boundary of the model.

one of the most important applications of the computer model presented in this paper will be to design field surveys. The large anomalies computed for a conductive zone within a deeply buried resistive layer illustrate the potential usefulness of hole-to-surface resistivity measurements for hazardous waste disposal problems.

References

Alfano, Luigi, 1962, Geoelectrical prospecting with underground electrodes: Geophys. Prosp., v. 10, p.290-303.

Ames, W.F., 1977, Numerical methods for partial differential equations: Academic Press, New York.

Anderson, W.L., 1975, Improved digital filters for evaluating Fourier and Hankel transform integrals: NTIS PB-242 800, Springfield, Va.

Carre, B.A., 1961, The determination of the optimum accelerating factor for successive over-relaxation: Computer Journal, V. 4, p. 73-78.

Dakhnov, V.N., 1959, Geophysical well logging: Quart. Colo. School of Mines, v. 57, 443 p. (translation by G.V. Keller).

Daniels, 1977, Three-dimensional resistivity and induced-polarization modeling using buried electrodes: Geophysics, V. 42, p. 1006-1019.

Daniels, J.J., 1978, Interpretation of buried electrode resistivity data using a layered earth model: Geophysics, v. 43, p. 988-1011.

Daniels, J.J., 1982, Hole-to-surface resistivity measurements at Gibson Dome (drill hole GD-1): U.S. Geological Survey Open File Report 82-320.

Dey, A., and Morrison, H.F., 1976, Resistivity modeling for arbitrarily shaped two-dimensional structures, Parts I and II: Lawerence Berkeley Laboratory Report no. LBL-5223.

Dey, A., and Morrison, H.F.,1979, Resistivity modeling for arbitrarily shaped three-dimensional structures: Geophysics, v. 44, p. 753-780.

Gunn, J.E., 1964, The numerical solution of $Au = f$ by semi-explicit alternating direction iterative method: Numer. Math., v. 6, p. 181-196.

Holcombe, H.T., 1982, Terrain effects in resistivity and magnetotelluric surveys: U.S. Department of Energy Report no. DOE/ID/12038-T1.

Holcombe, H.T. 1983, Three-dimensional isoparametric finite element computer algorithm for surface and down-hole DC resistivity applications -- fortran algorithm RES3TA: Report on Contract No. 138339-83 for U.S. Geological Survey.

Huebner, K.H., 1975, The finite element method for engineers: John Wiley and Sons, New York.

Merkel, R.H., 1971, Resistivity analysis for plane-layer halfspace models with buried current sources: Geophys. Prosp., v. 19, p. 626-639.

Merkel, R.H., and Alexander, S.S., 1971, Resistivity analysis for models of a sphere in a halfspace with buried current sources: Geophys. Prosp., v. 19, p. 640-651.

Mikhlin, S.G., and Smolitskiy, K.L., 1967 Approximate methods for solution of differential and integral equations: Elsevier, New York..

Norrie, D.H., and de Vries, G., 1978,An introduction to finite element analysis: Academic Press, New York.

Pridmore, D.F., 1978, Three-dimensional modeling of electric and electromagnetic data using the finite element method: Ph.D. Dissertation, Univ. of Utah, Salt Lake City, Utah.

Pridmore, D.F., Hohmann, G.W., Ward, S.H., and Sill, W.R., 1981, An investigation of finite element modeling for electrical and electromagnetic data in three-dimensions: Geophysics, v. 46, p. 1009-1024.

Snyder, D.D., and Merkel, R.M., 1973, Analytic models for the interpretation of electrical surveys using buried current electrodes: Geophysics, v. 46, p. 1009-1024.

Van Norstrand, R.G., and Cook, K.L., 1966, Interpretation of resistivity data: U.S. Geological Survey Professional Paper 499.